WILEY-VCH

DOI: 10.1002/((please add manuscript number))

Article type: Communication

A Low Reabsorbing Luminescent Solar Concentrator Employing π-Conjugated Polymers

Gregory D. Gutierrez, Igor Coropceanu, Moungi G. Bawendi, and Timothy M. Swager**

G. D. Gutierrez, I. Coropceanu, Prof. M. G. Bawendi,* Prof. T. M. Swager*
Department of Chemistry, Massachusetts Institute of Technology, Cambridge, MA 02139, USA
E-mail: tswager@mit.edu, mgb@mit.edu

Keywords: luminescent solar concentrators, π-conjugated polymers, energy transfer

To increase the viability of solar radiation as a widespread and accessible class of renewable energy, researchers are actively developing solutions to lower the cost of deploying highly efficient photovoltaic (PV) devices. One widely investigated approach is to use a platform capable of focusing solar energy onto a set of small, but efficient PV cells. The most convenient example of this approach is the luminescent solar concentrator (LSC), which has the advantage that it is compatible with typical infrastructures.[1–4] LSCs consist of transparent plastic or glass waveguides that channel luminophore photoemission from the absorption of sunlight to much smaller PV cells attached at their edges.[5] Although a promising architecture as a result of the ability to effectively collect sunlight without tracking the sun, conventional LSCs are often plagued by a multitude of unfavorable processes that curb their ability to deliver light to PV cells.[3] Of these limitations, non-radiative reabsorption by the luminophores is regarded as one of the most severe problems and results from significant overlap of the molecule's absorption and emission spectra.[6] Thus, although luminophores with high photoluminescence quantum yields (Φ_{PL}) such as perylene bisimides are desired,[7,8] their performance in LSCs will suffer if they possess small Stokes shifts.

A general approach to reducing reabsorption by molecules with narrow Stokes shifts, such as a perylene bisimide, is to employ minimal concentrations of luminophore such that its probability of encountering an emitted photon en route to the edges of the LSC is low.[9] This tactic, however, comes at the cost of poor light harvesting by the emitter. To overcome this drawback and power the coupled PV cells, one or more strongly absorbing luminescent species can be added to the LSC to enhance the minority perylene bismide's emission through energy transfer processes. Materials that have been recently investigated in an analogous manner are semiconducting heterostructured quantum dots[10–12] and rods[13] wherein the excitons of a higher gap CdS shell are efficiently shuttled to a highly luminescent lower gap CdSe core with a much smaller absorption cross-section, resulting in a separated absorption spectrum primarily resembling that of the shell and an emission entirely attributed to the core. Although organic luminophore-based LSCs that exploit energy transfer schemes to broaden the absorption of an acceptor are also well documented,[14–16] those aimed at specifically reducing reabsorption through the use of minority emitters have relied on a limited set of dyes[17,18] and biological motifs.[19] The extension of this strategy to discover the untapped potential of any powerful organic emitter with a very small Stokes shift, especially one as prized as a perylene bisimide, remains as a challenge.

As highly delocalized semiconducting macromolecular wires, π-conjugated polymers accommodate fast exciton migration along their backbones that may be easily disrupted by smaller quantities of lower gap emitters.[20] Such energy transfer may be accomplished through dipole-dipole coupling mechanisms (i.e. Förster resonance energy transfer, or FRET) between a luminescent polymer and a minority emitter with significant spectral overlap between the emission of the donor and absorption of the acceptor.[21] However, our laboratory has demonstrated that thin films of poly(arylene ethynylene)s (PAEs) may participate in electron exchange energy transfer processes (i.e. the Dexter mechanism) that circumvent this requirement and amplify the emission of spectrally mismatched fluorescent far red dyes.[22] We

hypothesized that a combination of two luminescent PAEs of different optical bandgaps (E_g) may cooperate in an excitonic relay with a red-emitting perylene bisimde through both FRET and electron exchange processes (**Figure 1**, a, b). Furthermore, through bandgap tuning of the polymers and judicious selection of the minority red emitter, the absorption spectra of both polymers can be decoupled from the emission of the terminal species while still exhibiting strong absorption across the visible spectrum.

To demonstrate the promise of this proposed down-conversion, we describe herein a highly emissive, low reabsorbing thin film LSC that makes use of a migratory excitonic cascade from PAEs **P1** ($E_g \approx 2.7$ eV) and **P2** ($E_g \approx 2.3$ eV) to minority perylene bisimide Lumogen F Red 305 (**Red 305**, $E_g \approx 2.0$ eV), the structures of which are displayed in Figure 1c. As the efficiencies of both FRET and electron exchange highly depend on the distance between donor and acceptor,[23] a core requirement necessary to effectively activate all modes of energy transfer in this ternary scheme is to keep all participants in the cascade proximate to each other. An ideal configuration involves hosting the minority emitter in a layer of **P1** and **P2**. To accomplish this we needed to address the tendency of π-conjugated polymers to undergo aggregation-induced luminescence quenching that impedes energy transfer to the high Φ_{PL} minority luminophore.[24] To overcome this problem, we utilized bulky *tert*-butylated pentiptycene units to render the polymers' backbones incapable of simple and direct π-π stacking. **P1**[25] and **P2**[26] are structurally modified derivatives of PAEs previously studied by our laboratory and were synthesized via the Sonogashira cross coupling reaction (see Supporting Information). As a result of their inability to undergo interchain π-π stacking and alkyl substituents in their repeat units, these PAEs have high solubility for mixing with other polymers and casting into thin films. The absorption and emission spectra of thin films of **Red 305** in poly(methyl methacrylate) (PMMA) and the individual PAEs are displayed in Figure 1d. Although both **P1** and **P2** possess small Stokes shifts, there is no overlap

between their absorption and the emission of **Red 305**, thereby supporting the directed energy transfer cascade.

The schematic of the LSC is illustrated in **Figure 2** (a). The device is a 50/50 blend of **P1** and **P2** that functions as the host matrix for small amounts of **Red 305** as the terminal isotropic emitter. The resulting thin film composite lies on a thick transparent square substrate that acts as the primary waveguiding medium. The latter feature is best realized with a host layer refractive index that is nearly equal to or lower than the substrate at the relevant emission wavelengths.[19] Consequently, the corresponding light guided to the edges of the LSC will be primarily confined to the substrate, thereby avoiding reabsorption. To obtain the refractive index n as a function of wavelength (Figure 2b), we applied spectroscopic ellipsometry to model the dielectric function of a host layer consisting of 1:1 (by weight) **P1**:**P2** (see Supporting Information). The wavelength profile of n exhibits wide dispersion that is typical of thin films of semiconducting π-conjugated polymers:[27] n ranges as low as 1.58 in the absorptive regime and as high as about 1.70 in the emissive region of the blend. Within the photoluminescence of **Red 305** (λ = 545 nm to λ = 800 nm), n ranges from 1.65 to 1.61. Guided by this data, we used N-SF10 glass ($n \approx 1.7$) as a compatible substrate, although polycarbonate is also a potential candidate ($n \approx 1.6$). It is worth noting that the refractive indices of π-conjugated polymer films often depend on the thickness and processing conditions of the film.[28] Thus, the data in Figure 2b is best translated to the LSC if similar processing conditions are observed. Nonetheless, by design n is relatively low for π-conjugated polymer films containing highly polarizable benzo[2,1,3]thiadiazoles as repeat units[29] and this is the result of the large internal free volume provided by the *tert*-butylated pentiptycene scaffold.[30]

LSC1 was constructed by spin casting an optically clear blend of 1:1 (by weight) **P1**:**P2** containing 1.5 wt% **Red 305** on top of a square piece of N-SF10 glass with dimensions 17.5 mm x 17.5 mm x 1.5 mm (**Figure 3**). The geometric gain (G), or the ratio of the area of a single face of the LSC to the total

area of edges coupled to a PV device, represents the concentrating capability of the LSC. Assuming all four edges will be completely covered by PV cells, the value of *G* for **LSC1** is approximately 3. The measured film thickness of **LSC1** (186.2 nm) is close to that of the ellipsometry sample and thus correlates with the data in Figure 2b. As a result of its small amount, **Red 305** was assumed to not affect *n*.

The absorption and photoluminescence spectra of **LSC1** is displayed in Figure 3a.[31] The two major bands that span λ = 400 nm to λ = 540 nm are attributed to **P1** and **P2**, whereas the much smaller peak centered at λ = 564 nm is assigned to the minority **Red 305** present. To directly quantify the amount of light absorbed at a given wavelength, the absorption spectrum is displayed in the form of its absorptance, which corresponds to the fraction of incident light absorbed after correcting for reflection (i.e. absorptance = $1 - 10^{-A}$, where *A* is the measured absorbance). **LSC1** absorbs approximately 70% of light at its absorption maximum (λ_{max} = 422 nm) and as much as 40% around λ = 500 nm. In contrast to these larger magnitudes, the peak absorption of **Red 305** is only about 2%. However, upon excitation of **LSC1** in a regime where absorption is mainly attributed to **P1** (i.e. λ_{ex} = 405 nm), the photoluminescence spectrum almost completely resembles that of **Red 305** with minor residual emission from **P2** present.

The total Φ_{PL} of **LSC1** was evaluated with an integrating sphere and measured with an excitation wavelength of λ_{ex} = 405 nm, which is close to the absorption maximum. For **LSC1**, Φ_{PL} was determined to be 79%, among the highest values observed for π-conjugated polymer thin films.[32] Following precedent for other systems,[14,18] a portrait of the efficiency of energy transfer (η_{ET}) from the PAEs to **Red 305** was then determined. An excitation spectrum was acquired via monitoring an emission wavelength of λ_{em} = 630 nm, which should be effectively attributed to **Red 305** (Figure 3b). From this data, η_{ET} from **P1** and **P2** to **Red 305** per wavelength was calculated as the ratio of the normalized excitation intensity to the normalized absorptance (Figure 3c). The spectra are normalized at the

absorption maximum of the minority **Red 305** to assign a default η_{ET} of 100%. Within the higher-energy band (λ = 400 nm to λ = 460 nm), η_{ET} maintains values between 88% and 80%, while efficiencies for the second band (λ = 460 nm through λ = 525 nm) vary from 80% to 62%. By invoking the Kasha-Vavilov rule for **LSC1**, Φ_{PL} from **Red 305** ($\Phi_{PL,R}$) as a function of excitation wavelength may then be estimated with Equation 1.

$$\Phi_{PL,R}(\lambda) = \Phi^{\circ}_{PL}\left(\frac{F_R}{F_{total}}\right)\left(\frac{\eta_{ET}(\lambda)}{\eta^{\circ}_{ET}}\right) \quad (1)$$

Where Φ°_{PL} and η°_{ET} are the total quantum yield and energy transfer efficiency at λ_{ex} = 405 nm, respectively. F_R/F_{total} is the fraction of the area under the emission spectrum (Figure 3a) that is assigned to **Red 305** (i.e. between λ = 545 nm and λ = 800 nm) due to the very small contribution from **P2**. This ratio indicates that, with λ_{ex} = 405 nm, this region is responsible for about 88% of the observed photoluminescence. Through Equation 1, the plot of $\Phi_{PL,R}$ with excitation wavelength indicates that **Red 305** maintains quantum yields near or above 50% at all wavelengths via energy transfer by **P1** and **P2** (Figure 3c).

The key metric of an LSC's performance is its optical efficiency (η_{opt}), defined as the fraction of incident photons emanating from the edges of the device. As a key goal of LSC research is to scale developed prototypes to commercially relevant sizes, we applied a Monte Carlo simulation to assess the promise of larger versions of our designed LSC by calculating η_{opt} as a function of G through an analysis of unproductive loss channels. Figure 4 summarizes these results using the photophysical data in Figure 3a, the total Φ_{PL}, and an assumed refractive index of 1.7 across all emission wavelengths as inputted parameters for **LSC1**. For **LSC1**, η_{opt} was calculated as approximately 40%. A plot of η_{opt} versus G (Figure 4a) exhibits a slow and steady decrease as G increases, an expected trend due to non-radiative reabsorption by the trace absorption of **Red 305**. Despite this drop, scaled versions of **LSC1** are projected to maintain high η_{opt} at large G and is well above 20% even at G = 400, on par with predictions for high-performing nanocrystal LSCs.[33] The concentration factor, or the product of G and

η_{opt}, is also plotted as a function of G and represents the actual magnitude of photon concentration by the LSC and rises in a nearly linear fashion as G increases. For example, at G = 400, a 90-fold concentration of photons toward PV cells at the edges is expected.

Figure 4b summarizes the simulation's calculated impact of the possible loss mechanisms on the performance of **LSC1** at G = 200 and a single excitation wavelength (λ_{ex} = 405 nm). The displayed chart tabulates the fates of incident photons that strike the face of the scaled LSC. Prior to absorption, the fixed Fresnel coefficient for the inputted refractive index directly contributes to a 7% loss of photons via reflection off the surface of the LSC. By taking into account that some incident photons are lost due to incomplete absorption by the LSC after this reflection occurs ("Not Absorbed," 31%), the simulation predicts non-radiative events ("Not Reemitted") to result in a modest 21% loss in which minor reabsorption processes play a large role. Additionally, a leakage of emitted photons through the waveguide's escape cone ("Top Loss") is projected to result in a 15% overall loss. The remaining 27% of incident photons, albeit down-converted by **Red 305** ("Collected"), represents η_{opt}.

To summarize, we have demonstrated a blend of π-conjugated polymers as amplifying antennae for a perylene bisimide to create a low reabsorbing thin film LSC with significant absorption in the visible spectrum and performance similar to state-of-the-art analogs. The participants of the described cascade all possess solubilities that allow for facile and low-cost solution processing. Through the development of even lower gap luminescent π-conjugated polymers, we envision creating additional high-performance LSCs capable of more complete absorption of the visible spectrum with efficient energy transfer directed toward spectrally separated minority terminal luminophores that emit in the far red or near-infrared for improved spectral matching with silicon PV cells.

Supporting Information

Supporting Information is available from the Wiley Online Library or from the author.

Acknowledgements

This work was sponsored by Eni S.p.A. as part of the efforts of the MIT-Eni Solar Frontiers Alliance. Both G. D. G. and I. C. gratefully acknowledge support from the National Science Foundation Graduate Research Fellowship Program (Grant Number 1122374). We thank Lionel Moh for assistance with spectroscopic ellipsometry and Phil Reusswig and Tony Wu for initial assistance with integrating sphere measurements.

[1] B. C. Rowan, L. R. Wilson, B. S. Richards, *IEEE J. Sel. Top. Quantum Electron.* **2008**, *14*, 1312.

[2] W. G. J. H. M. van Sark, K. W. J. Barnham, L. H. Slooff, A. J. Chatten, A. Büchtemann, A. Meyer, S. J. McCormack, R. Koole, D. J. Farrell, R. Bose, E. E. Bende, A. R. Burgers, T. Budel, J. Quilitz, M. Kennedy, T. Meyer, C. D. M. Donegá, A. Meijerink, D. Vanmaekelbergh, *Opt. Express* **2008**, *16*, 21773.

[3] M. G. Debije, P. P. C. Verbunt, *Adv. Energy Mater.* **2012**, *2*, 12.

[4] Selected examples of architectures: a) J. S. Batchelder, A. H. Zewail, T. Cole, *Appl. Opt.* **1981**, *20*, 3733; b) V. Sholin, J. D. Olson, S. A. Carter, *J. Appl. Phys.* **2007**, *101*, 123114; c) L. H. Slooff, E. E. Bende, A. R. Burgers, T. Budel, M. Pravettoni, R. P. Kenny, E. D. Dunlop, A. Büchtemann, *Phys. Status Solidi RRL* **2008**, *2*, 257; d) N. C. Giebink, G. P. Wiederrecht, M. R. Wasielewski, *Nature Photon.* **2011**, *5*, 694.

[5] For an alternative approach, see: J. Yoon, L. Li, A. V. Semichaevsky, J. H. Ryu, H. T. Johnson, R. G. Nuzzo, J. A. Rogers *Nat. Commun.* **2011**, *2*, 343.

[6] O. M. ten Kate, K. M. Hooning, E. van der Kolk, *Appl. Opt.* **2014**, *53*, 5238.

[7] F. Würthner, *Chem. Commun.* **2004**, 1564.

[8] W. E. Benjamin, D. R. Veit, M. J. Perkins, E. Bain, K. Scharnhorst, S. McDowall, D. L. Patrick, J. D. Gilbertson, *Chem. Mater.* **2014**, *26*, 1291.

[9] L. R. Wilson, B. C. Rowan, N. Robertson, O. Moudam, A. C. Jones, B. S. Richards, *Appl. Opt.* **2010**, *49*, 1651.

[10] I. Coropceanu, M. G. Bawendi, *Nano Lett.* **2014**, *14*, 4097.

[11] F. Meinardi, A. Colombo, K. A. Velizhanin, R. Simonutti, M. Lorenzon, L. Beverina, R. Viswanatha, V. I. Klimov, S. Brovelli, *Nature Photon.* **2014**, *8*, 392.

[12] L. R. Bradshaw, K. E. Knowles, S. McDowall, D. R. Gamelin, *Nano Lett.* **2015**, *15*, 1315.

[13] N. D. Bronstein, L. Li, L. Xu, Y. Yao, V. E. Ferry, A. P. Alivisatos, R. G. Nuzzo, *ACS Nano* **2014**, *8*, 44.

[14] B. A. Swartz, T. Cole, A. H. Zewail, *Opt. Lett.* **1977**, *1*, 73.

[15] S. T. Bailey, G. E. Lokey, M. S. Hanes, J. D. M. Shearer, J. B. McLafferty, G. T. Beaumont, T. T. Baseler, J. M. Layhue, D. R. Broussard, Y.-Z. Zhang, B. P. Wittmershaus, *Sol. Energ. Mat. Sol. Cells* **2007**, *91*, 67.

[16] O. A. Bozdemir, S. Erbas-Cakmak, O. O. Ekiz, A. Dana, E. U. Akkaya, *Angew. Chem. Int. Ed.* **2011**, *50*, 10907.

[17] M. J. Currie, J. K. Mapel, T. D. Heidel, S. Goffri, M. A. Baldo, *Science* **2008**, *321*, 226.

[18] J. L. Banal, K. P. Ghiggino, W. W. H. Wong, *Phys. Chem. Chem. Phys.* **2014**, *16*, 25358.

[19] C. L. Mulder, L. Theogarajan, M. Currie, J. K. Mapel, M. A Baldo, M. Vaughn, P. Willard, B. D. Bruce, M. W. Moss, C. E. McLain, J. P. Morseman, *Adv. Mater.* **2009**, *21*, 3181.

[20] T. M. Swager, C. J. Gil, M. S. Wrighton, *J. Phys. Chem.* **1995**, *99*, 4886.

[21] Z. Tian, J. Yu, C. Wu, C. Szymanski, J. McNeill, *Nanoscale* **2010**, *2*, 1999.

[22] M. Levine, I. Song, T. L. Andrew, S. E. Kooi, T. M. Swager, *J. Polym. Sci. A Polym. Chem.* **2010**, *48*, 3382.

[23] E. V. Anslyn, D. A. Dougherty, *Modern Physical Organic Chemistry*, University Science Books, Sausalito, CA, USA **2006**.

[24] S. A. Jenekhe, J. A. Osaheni, *Science* **1994**, *265*, 765.

[25] J.-S. Yang, T. M. Swager, *J. Am. Chem. Soc.* **1998**, *120*, 11864.

[26] J. Bouffard, T. M. Swager, *Macromolecules* **2008**, *41*, 5559.

[27] C. M. Ramsdale, N. C. Greenham, *Adv. Mater.* **2002**, *14*, 212.

[28] M. Campoy-Quiles, G. Heliotis, R. Xia, M. Ariu, M. Pintani, P. Etchegoin, D. D. C. Bradley, *Adv. Funct. Mater.* **2005**, *15*, 925.

[29] C. M. Ramsdale, N. C. Greenham, *J. Phys. D: Appl. Phys.* **2003**, *36*, L29.

[30] T. M. Long, T. M. Swager, *J. Am. Chem. Soc.* **2003**, *125*, 14113.

[31] The absorption spectrum was corrected for minor thin film interference effects in the transparent region by correcting the baseline at λ = 650 nm. Through this correction, a logarithmic view of the photophysical spectra reveals the measured absorbance at the emission maximum (λ_{ex} = 595 nm) to be approximately 500 times smaller than that at the absorption maximum (Figure S17).

[32] a) B. R. Hsieh, Y. Yu, E. W. Forsythe, G. M. Schaaf, W. A. Field, *J. Am. Chem. Soc.* **1998**, *120*, 231; b) C. Ego, D. Marsitzky, S. Becker, J. Zhang, A. C. Grimsdale, K. Müllen, J. D. MacKenzie, C. Silva, R. H. Friend, *J. Am. Chem. Soc.* **2003**, *125*, 437; c) J.-S. Kim, R. H. Friend, I. Grizzi, J. H. Burroughes, *Appl. Phys. Lett.* **2005**, *87*, 023506; d) A. J. Cadby, R. Dean, C. Elliott, R. A. L. Jones, A. M. Fox, D. G. Lidzey, *Adv. Mater.* **2007**, *19*, 107. e) U. Giovanella, C. Botta, F. Galeotti, B. Vercelli, S. Battiato, M. Pasini, *J. Mater. Chem. C* **2013**, *1*, 5322.

[33] C. S. Erickson, L. R. Bradshaw, S. McDowall, J. D. Gilbertson, D. R. Gamelin, D. L. Patrick, *ACS Nano* **2014**, *8*, 3461.

Received: ((will be filled in by the editorial staff))
Revised: ((will be filled in by the editorial staff))
Published online: ((will be filled in by the editorial staff))

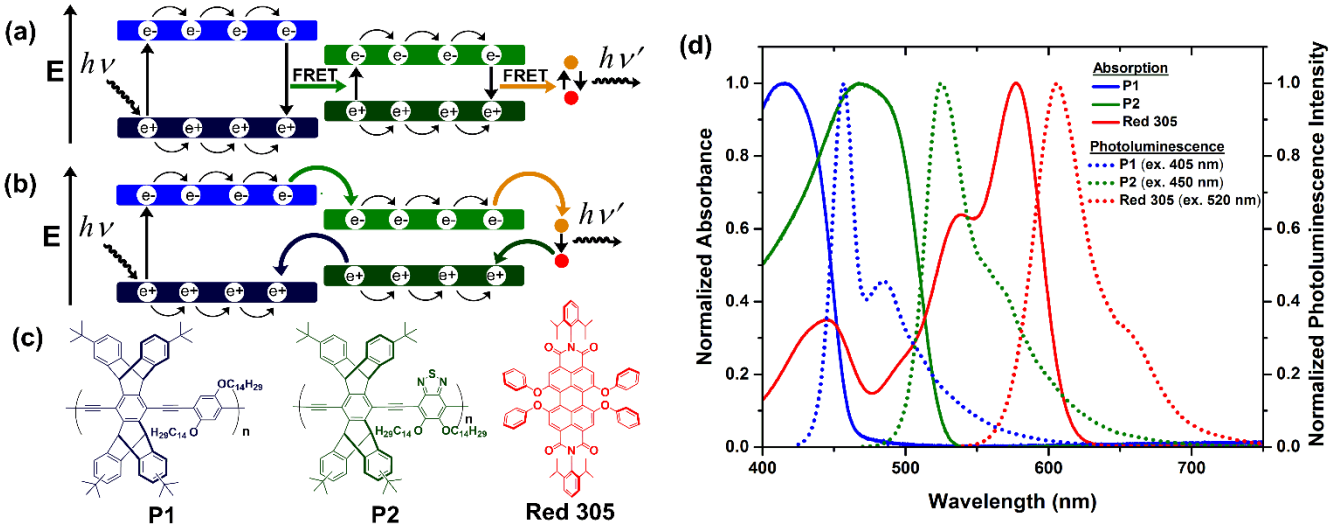

Figure 1. Photoinduced migratory cascade of excitons in thin films of two π-conjugated polymers, **P1** (blue) and **P2** (green), to minority fluorophore **Red 305** (red) via (a) FRET and (b) electron exchange (Dexter) energy transfer. (c) Structures of **P1**, **P2**, and **Red 305**. (d) Absorption (solid) and emission (dashed) spectra of thin films of **P1** (blue) and **P2** (green) and a sample of 0.5 wt% **Red 305** in PMMA (red). Optical bandgaps were estimated from absorption onsets.

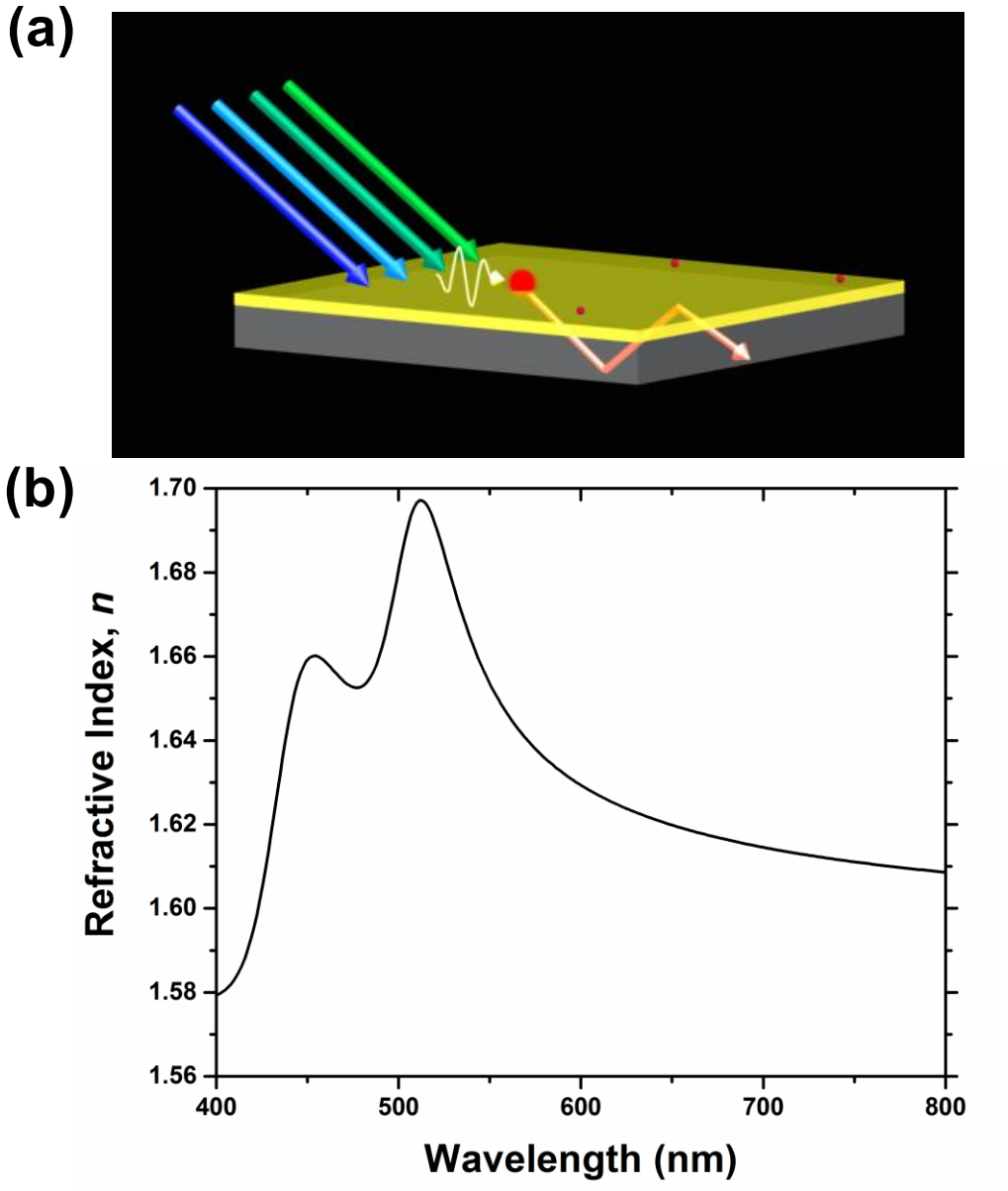

Figure 2. (a) Schematic of the designed LSC (yellow layer: blend of **P1** and **P2**; red: molecule of **Red 305**) illustrating exciton diffusion from **P1** and **P2** to **Red 305**. (b) Refractive index (*n*) of a film of 1:1 (by weight) **P1**:**P2** (thickness = 188.3 nm).

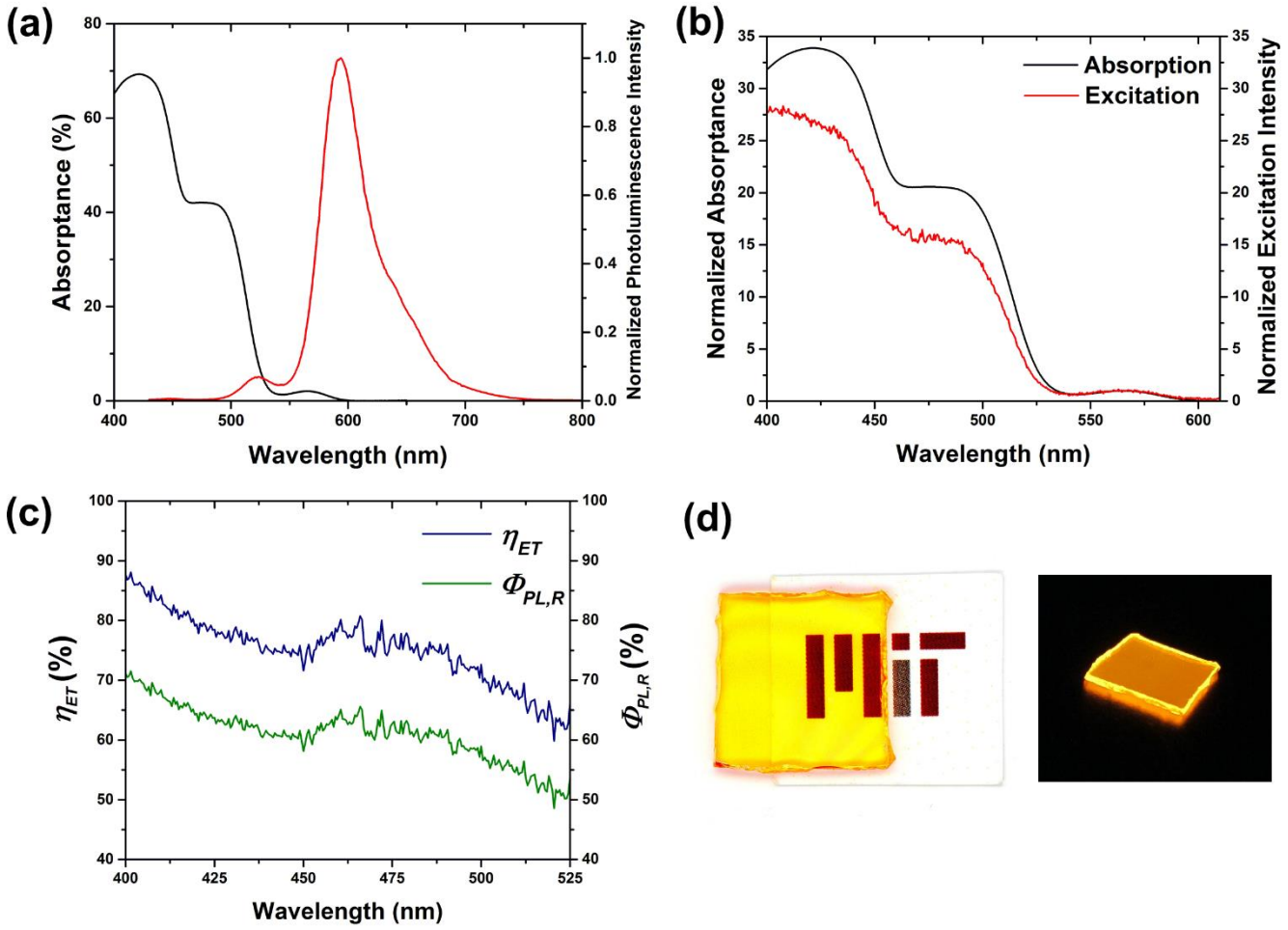

Figure 3. (a) Absorption and emission (λ_{ex} = 405 nm) spectra of **LSC1** with absorption in terms of its absorptance. (b) Absorption and excitation spectra (λ_{em} = 630 nm) of **LSC1** normalized at λ = 564 nm. (c) Plots of the energy transfer efficiency (η_{ET}) from **P1** and **P2** to **Red 305** and estimated photoluminescence quantum yield of **Red 305** ($\Phi_{PL,R}$) in **LSC1** with respect to wavelength. (d) **LSC1** under normal lighting (left) and UV radiation at λ = 365 nm to illustrate light concentration at the edges (right).

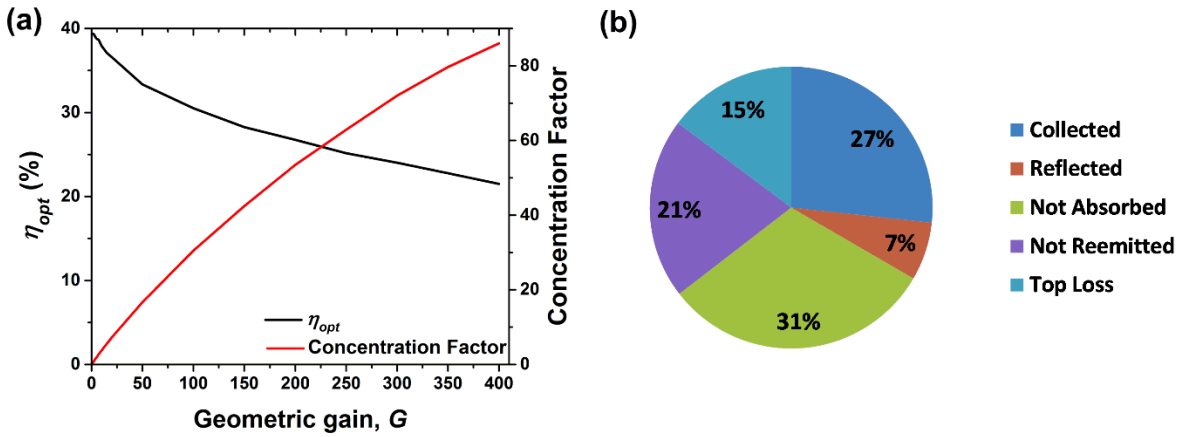

Figure 4. (a) Projected optical efficiency (η_{opt}) and concentration factor with increasing geometric gain (G) for **LSC1**. (b) Calculated loss channels for G = 200 (λ_{ex} = 405 nm).

Abstract

A highly efficient thin film luminescent solar concentrator (LSC) utilizing two π-conjugated polymers as antennae for small amounts of the valued perylene bisimide Lumogen F Red 305 is presented. The LSC exhibits high photoluminescence quantum yield, low reabsorption, and relatively low refractive indices for waveguide matching. A Monte Carlo simulation predicts the LSC to possess exceptionally high optical efficiencies on large scales.

Keyword: luminescent solar concentrators, photovoltaics, conjugated polymers, energy transfer

Gregory D. Gutierrez, Igor Coropceanu, Moungi G. Bawendi, and Timothy M. Swager*

A Low Reabsorbing Luminescent Solar Concentrator Employing π-Conjugated Polymers

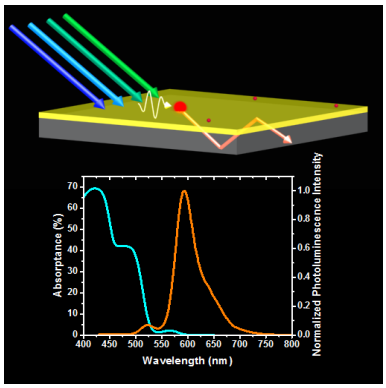

Supporting Information

A Low Reabsorbing Luminescent Solar Concentrator Employing π-Conjugated Polymers

*Gregory D. Gutierrez, Igor Coropceanu, Moungi G. Bawendi, and Timothy M. Swager**

I. General information

A. Materials

Prior to use, *N*,*N*-diisopropylamine was distilled over KOH and sparged under argon for 1 hour. Toluene was passed through a solvent purification system (SPS) via columns of activated alumina, stored over 3 Å molecular sieves, and sparged under argon for 1 hour. Anhydrous THF was also obtained from the same SPS and used immediately. Unless otherwise indicated, all other purchased solvents and reagents were used without additional purification. Lumogen F Red 305 was obtained from BASF and also used without further purification. Column chromatography was implemented with silica gel (60 Å pore size, 230 – 400 mesh, Sigma-Aldrich) as the solid phase. Thin layer chromatography (TLC) was carried out with Baker-flex silica gel IB-F plates (J. T. Baker). N-SF10 glass samples (Schott) were obtained as circular blank plates (25 mm diameter, 1.5 mm thickness) from UQG Optics (Cambridge, UK) and manually cut to specification with a diamond cutter. The glass was cleaned with acetone and chloroform, followed by a stream of N_2 gas, before use.

B. Instrumentation and measurements

^{1}H NMR (400 MHz) and ^{13}C NMR (101 MHz, proton-decoupled) spectra were acquired using a Bruker Avance III HD NMR spectrometer. The multiplicities and/or shape of all indicated resonances are labeled with the following key: singlet (“s”), doublet (“d”), doublet of doublets (“dd”), triplet (“t”), multiplet (“m”), and broad (“br.”). All spectra were obtained with $CDCl_3$ as the

solvent and reported chemical shifts are referenced with respect to solvent peaks (δ = 7.26 ppm for ^{1}H and δ = 77.16 ppm for ^{13}C). NMR data for π-conjugated polymers are reported in the context of a single repeat unit. Gel permeation chromatography (GPC) measurements were carried out using an Agilent 1260 Infinity gel permeation chromatograph with UV/vis and refractive index detectors calibrated against polystyrene standards and THF as the eluent. The injection concentration of the prepared GPC samples was 0.5 mg/mL. High resolution mass spectrometry (HRMS) data were obtained via direct analysis in real time (DART) with positive ionization at the MIT Department of Chemistry Instrumentation Facility with a Bruker Daltronics APEXIV 4.7 Tesla FT-ICR mass spectrometer. Mass spectrometry (MS) via matrix assisted laser desorption/ionization-time of flight (MALDI-TOF) was performed at the MIT Biopolymers Laboratory using 2,5-dihydroxybenzoic acid as the matrix. Melting point determination was carried out with a MelTemp II melting point apparatus (Laboratory Devices Inc, USA). Spin coated samples were created using a Model WS-400 Spin Processor (Laurel Technologies Corporation) coupled to a vacuum line. Film thicknesses were measured using a Dektak 6M profilometer. Ellipsometry measurements were carried out using a J. A. Woollam Co., Inc. M-2000D variable angle spectroscopic ellipsometer and the V.A.S.E. 32 software package.

Photophysical spectra were obtained with thin films facing the source lamps. Absorption spectra were obtained using an Agilent Cary 4000 UV/vis spectrophotometer. Photoluminescence and excitation spectra were acquired on a HORIBA Jobin Yvon Fluorolog-3 spectrofluorometer (model FL-321) equipped with a 450 W xenon lamp as the excitation source. Front-face detection was used to observe photoluminescence near excitation.

Quantum yield measurements were taken using an integrating sphere (Labsphere RTC-060-SF). The experimental set-up that was used is shown schematically in Figure S1 below. The sample was illuminated using a 405 nm diode laser with an excitation power of 5mW that was chopped at 210

Hz. The output was collected using a calibrated germanium detector (Newport: 818-UV) through a Stanford Research Systems lock-in amplifying system. The integrating sphere included two baffles, one which lay immediately beneath the sample holder to prevent direct emission into the detector as well as a baffle on a side, which could be used to ensure that reflected light from the initial beam could only reach the detector after multiple reflection events.

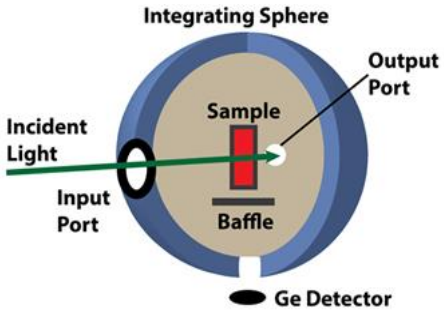

Figure S1. The configuration used to measure the absolute quantum yield.

Two measurements were than taken using this system: 1) Laser Intensity (LI), where the laser was directed behind one of the baffles with the sample outside of the sphere; 2) Sample Fluorescence (SF) where the excitation beam was passed through the sample and out through an exit port and the reflection was allowed to exit through the side port. From these two measurements and the absorbance of the sample, it was possible to extract the photoluminescence quantum yield (Φ_{PL}) of the LSC by calculating the number of photons absorbed and the number of photons emitted (Equation S1):

$$\Phi_{PL} = \frac{\frac{\mathrm{SF}}{\mathrm{EQE(S)}} / \frac{\mathrm{LI}}{\mathrm{EQE(L)}}}{Abs(L)}$$

Equation S1. Equation for calculating the photoluminescence quantum yield Φ_{PL}.

In the equation above, EQE(S) and EQE(L) refer to the external quantum efficiency (EQE) of the detector at the wavelength of the sample emission and of the excitation source, respectively, and Abs(L) is the absorptance of the sample at the excitation wavelength.

C. Preparation of thin films

Thin films of P1, P2, and Red 305 in PMMA: Thin films of **P1** and **P2** were spin casted onto soda-lime glass substrates from 20 mg/mL chloroform solutions at 2000 rpm for 45 seconds. A thin film of 0.5 wt% **Red 305** in PMMA was made by drop casting a chloroform solution containing 100 mg/mL PMMA and 0.5 mg/mL **Red 305** onto a soda-lime glass substrate.

Model LSC (LSC1): 0.2 mL of a 0.375 mg/mL solution of **Red 305** in chloroform was added to a vial containing 2.50 mg **P1** and 2.50 mg **P2**. After dissolution of the polymers, 0.1 mL of the resulting solution was drawn into a syringe and quickly added on top of a blank plate of N-SF10 glass spinning at 2000 rpm. Upon completion of the injection, the sample was spun at the same speed for 45 seconds.

II. Synthetic procedures

2,6-di-*tert*-butylanthracene (**3**),[S1] 6,10-di(*tert*-butyl)triptycene-1,4-quinone (**4**),[S2] 1,4-bis(tetradecyloxy)benzene (**6**),[S3] and 5,6-bis(tetradecyloxy)benzo[2,1,3]thiadiazole (**8**)[S4] were synthesized following published procedures.

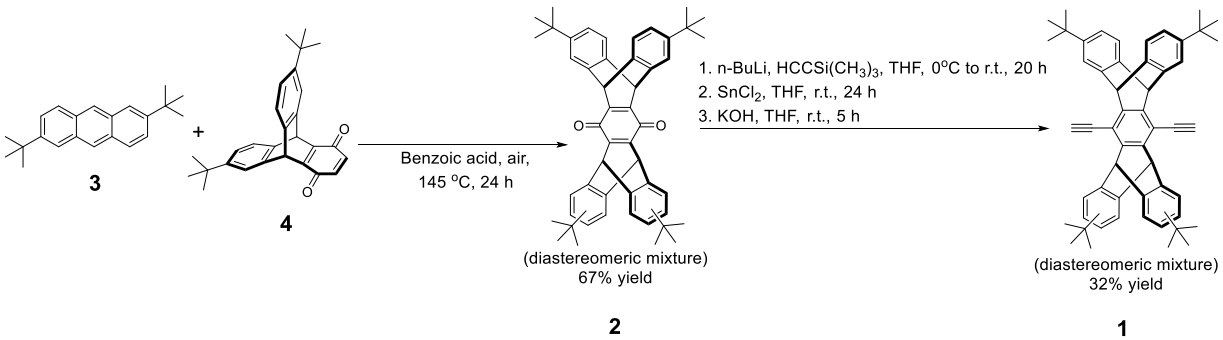

Scheme S1. Synthesis of *tert*-butylated pentiptycene dialkyne **1**.

tert-Butylated pentiptycene quinone **2**

The following synthesis is a modified preparation of **2** described in Nesterov et al.[S5] in which benzoic acid is employed as the solvent. To a 50 mL round bottom flask containing a magnetic stir bar, **3** (1.10 g, 3.79 mmol), **4** (1.88 g, 4.73 mmol), and benzoic acid (5.55 g, 45.5 mmol) were added and mechanically blended with a spatula. The flask was submerged in an oil bath heated to 145°C, a temperature at which benzoic melts, covered, and stirred under aerobic conditions. After 15 h, the reaction was quickly aerated and resealed with stirring proceeding for another 9 h. The reaction mixture was cooled to room temperature and the resulting solid slab was triturated into 2 x 30 mL $CHCl_3$. The fractions were combined and washed 2 x 100 mL saturated $NaHCO_3$ (*aq.*) solution, followed by 100 mL saturated NaCl (*aq.*) solution. The organic layer was dried with $MgSO_4$ and filtered. 15 g silica gel was added to the organic layer and volatiles were evaporated. The residue was dry-loaded at the top of a column of silica gel and purified using 100% hexanes as eluent to remove excess 2,6-di-*tert*-butylanthracene (**3**), followed by 1:1 $CHCl_3$:hexanes to obtain **2** as an orange solid and set of inseparable diastereomers (1.74 g, 67% yield). ^{1}H NMR (400 MHz, $CDCl_3$): δ (ppm) = 7.40 (d, 4H, J = 1.8 Hz, 4H), 7.28 (d, 4H, J = 7.8 Hz, 4H), 6.98 (dd, 4H, J_1 = 1.8 Hz, J_2 = 7.8 Hz, 4H), 5.70 (s, 4H), 1.22 (s, 36 H). ^{13}C NMR (101 MHz, $CDCl_3$): δ (ppm) = 180.5, 151.4, 148.8, 144.0, 141.0, 123.7, 122.0, 121.8, 47.4, 34.7, 31.6.

tert-Butylated pentiptycene dialkyne **1**

This procedure was performed with some modifications to the preparation of **1** described by Nesterov et al.[S5] To a solution of timethylsilylacetylene (1.00 g, 10.22 mmol, 1.44 mL) in 30 mL anhydrous THF at 0 °C were added *n*-BuLi (1.60 M in hexanes, 8.76 mmol, 5.47 mL) dropwise. The mixture was stirred at 0 °C under argon for 30 minutes and then cannula-transferred into a 500 mL 3-neck round bottom flask containing **2** (2.00 g, 2.92 mmol) in 200 mL anhydrous THF at 0 °C. The reaction was stirred at 0 °C for 1 h and then at room temperature for 18 h, all of which was under argon. The mixture was then poured into 100 mL 10% w/v NH_4Cl (*aq.*). 250 mL Et_2O was added and the biphasic mixture was partitioned. The organic layer was washed with 100 mL H_2O, then 100 mL saturated NaCl (*aq.*), dried with $MgSO_4$, and concentrated *in vacuo*. The crude residue was passed through a plug of silica gel using 1:1 $CHCl_3$:hexanes as the eluent. The crude mixture of diols was isolated as a beige solid and immediately dissolved in 50 mL THF (de-inhibited by distillation). The solution was sparged with argon for 25 minutes. A degassed solution of $SnCl_2{\cdot}2H_2O$ (1.65 g, 7.30 mmol) in 5 mL H_2O and 5 mL AcOH was cannula-transferred into the mixture and then stirred at room temperature under argon for 24 h. 20 mL of saturated $NaHCO_3$(*aq.*) solution was carefully added to neutralize the AcOH, followed by 25 mL H_2O. The resulting precipitate was filtered and washed with 10 mL saturated $NaHCO_3$ (*aq.*) solution and 10 mL H_2O. 100 mL $CHCl_3$ was added to the solid to dissolve any organic species with any remaining insoluble precipitates filtered off. The remaining solid was treated with another 100 mL $CHCl_3$, then filtered off. Both $CHCl_3$ fractions were combined and evaporated. The resulting crude material was subjected to column chromatography (3:7 $CHCl_3$:hexanes) to isolate 823 mg of a mixture of TMS-protected intermediates immediately carried over to the next step. (R_f = 0.41, 0.50 (SiO_2 TLC, 1:9 $CHCl_3$:hexanes)). The resulting solid was dissolved in 25 mL de-inhibited THF, to which a solution of KOH (106 mg, 1.89 mmol) in 10 mL MeOH was added. After stirring the reaction at room temperature for 3 h, the mixture was poured into 50 mL Et_2O, washed with 150 mL saturated NaCl

(*aq.*), 100 mL H_2O, and another 150 mL saturated NaCl (*aq.*) solution. The organic layer was dried with $MgSO_4$. To the filtered solution was added 5 g silica gel with volatiles then evaporated. The sample was dry-loaded onto a column of silica gel and chromatographed using a 1:9 $CHCl_3$:hexanes/1:1 $CHCl_3$:hexanes gradient to furnish 658 mg **1** as an off-white solid and mixture of diastereomers (32% overall yield). R_f = 0.34 (SiO_2 TLC, 1:9 $CHCl_3$:hexanes). ^{1}H NMR (400 MHz, $CDCl_3$): δ (ppm) = 7.39 (d, J = 1.8 Hz, 4H), 7.30-7.27 (2 d, J = 7.8 Hz, 4H), 6.97 (dd, 4H, J_1 = 1.8 Hz, J_2 = 7.8 Hz, 4H), 5.78 (s, 4H), 3.71-3.70 (2 s, 2H), 1.23 (s, 36H). ^{13}C NMR (101 MHz, $CDCl_3$): δ (ppm) = 148.4, 145.0, 142.20, 142.15, 123.3, 123.2, 121.96, 121.92, 121.3, 121.2, 114.01, 113.97, 84.43, 84.38, 79.60, 79.58, 52.0, 34.7, 31.6. MS (MALDI-TOF, m/z) calculated for $C_{54}H_{54}$, M^+: 702.423, found: 702.465. [S6]

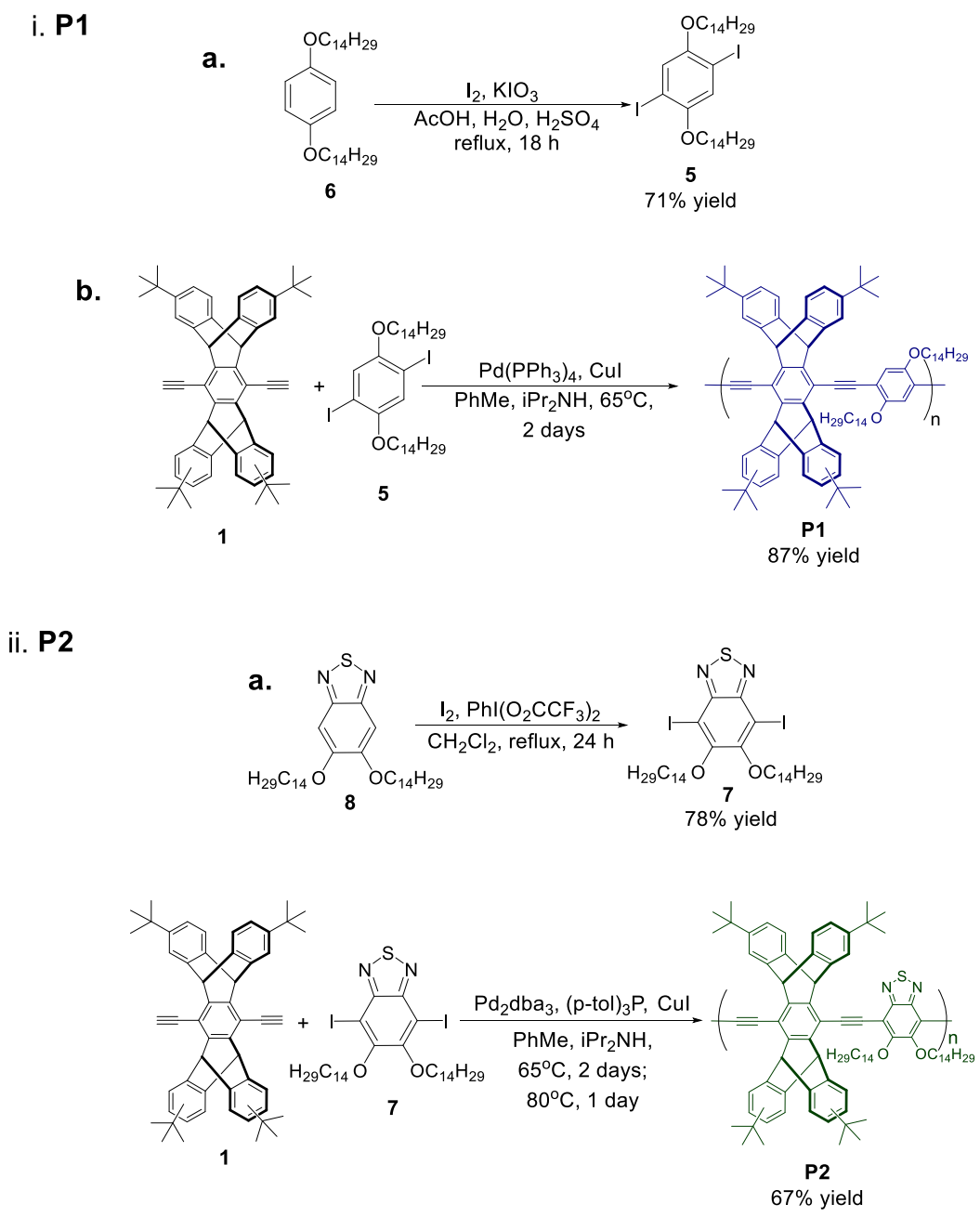

Scheme S2. Synthesis of π-conjugated polymers **P1** and **P2** from **1** and their respective bandgap-limiting co-monomers **5** and **7**.

2,5-diiodo-1,4-bis(tetradecyloxy)benzene (**5**)

Compound **5** was prepared with some modification to a general procedure offered for the synthesis of 2,5-diiodo-1,4-bis(alkoxy)benzenes.[S3] **6** (1.50 g, 2.98 mmol), I_2 (757 mg, 2.98 mmol), KIO_3 (319 mg 1.49 mmol), 30 mL AcOH, 3 mL H_2O, and 0.3 mL H_2SO_4 were added to a 100 mL round-bottom flask containing a magnetic stirbar and reflux condenser. The reaction was stirred at reflux for 18 h. 20 mL 10% $Na_2S_2O_3 \cdot 5H_2O$ (*aq*.) solution was then added to the flask. The mixture was added to 200 mL CH_2Cl_2 to dissolve the crude product and 100 mL H_2O. The organic layer was partitioned and then washed with 100 mL saturated $NaHCO_3$ (*aq*.) solution and 100 mL saturated NaCl (*aq*.) solution. The organic layer was dried with $MgSO_4$, filtered, and evaporated. The resulting residue was recrystallized from isopropanol twice to obtain **5** as a white solid (1.59 g, 71% yield). ^{1}H NMR (400 MHz, $CDCl_3$): δ (ppm) = 7.17 (s, 2H) 3.92 (t, J = 6.5 Hz, 4H), 1.80 (m, 4H), 1.49 (m, 4H), 1.26 (br. m, 40H) 0.88 (t, J = 7.1 Hz, 6H). ^{13}C NMR (101 MHz, $CDCl_3$): δ (ppm) = 153.0, 122.9, 86.5, 70.5, 32.1, 30.5, 29.9, 29.8, 29.7, 29.7, 26.1, 22.8, 14.3. HRMS (DART, m/z) calculated for $C_{34}H_{58}I_2N_2O_2S$, M^+: 754.2677, found: 754.2676.

4,7-Diiodo-5,6-bis(tetradecyloxy)benzo[2,1,3]thiadiazole (**7**)

The preparation of **7** is based on a procedure for the production of 4,7-diiodo-5,6-bis(octyloxy)benzo[2,1,3]thiadiazole reported by Nagarjuna et al.[S7] To a 300 mL round-bottom flask equipped with a magnetic stirbar were added **8** (2.50 g, 4.46 mmol), iodine (1.36 g, 5.35 mmol), [bis(trifluoroacetoxy)iodo]benzene (2.30 g, 5.35 mmol), and 150 mL CH_2Cl_2. A reflux condenser was attached to the flask and contents were heated to reflux and stirred for 24 hours. The reaction mixture was cooled to room temperature and washed with 2 x 100 mL 20% $Na_2S_2O_3$ (*aq*.) solution, 2 x 100 mL 20% $NaHCO_3$ (*aq*.) solution and 2 x 100 mL saturated NaCl (*aq*.) solution. The organic layer was dried with anhydrous $MgSO_4$ and filtered through a short plug of silica gel with CH_2Cl_2 as the eluent. The solvent was evaporated under reduced pressure and the resulting residue was recrystallized from isopropanol. The material was lastly subject to column chromatography

using 1:1 $CHCl_3$:hexanes as the eluent to furnish **7** as a white solid (2.83 g, 78% yield). R_f = 0.46 (SiO_2 TLC, 1:1 $CHCl_3$:hexanes). m.p. 81 °C – 82 °C. ^{1}H NMR (400 MHz, $CDCl_3$): δ (ppm) = 4.12 (t, J = 6.7 Hz, 4H), 1.91 (m, 4H), 1.54 (m, 4H), 1.26 (br. m, 40H) 0.88 (t, J = 7.1 Hz, 6H). ^{13}C NMR (101 MHz, $CDCl_3$): δ (ppm) = 157.2, 151.9, 82.8, 75.1, 32.1, 30.5, 29.9-29.8, 29.6, 29.5, 26.3, 22.8, 14.3. HRMS (DART, m/z) calculated for $C_{34}H_{58}I_2N_2O_2S$, $[M + H]^+$: 813.2381, found: 813.2367.

*π-Conjugated polymer **P1***

To a 25 mL Schlenk flask equipped with a magnetic stirbar were added **1** (300 mg, 0.427 mmol), **5** (349 mg, 0.469 mmol), $Pd(PPh_3)_4$ (24.66 mg, 21.34 μmol), and CuI (4.06 mg, 21.34 μmol). After degassing the flask with 3 vacuum-argon backfill cycles, 7 mL of degassed toluene and 3 mL of degassed *N*,*N*-diisopropylamine were added. The reaction mixture was stirred under argon at 65 °C for 2 days, which was then cooled to room temperature. The viscous mixture was then added dropwise to the vortex of 200 mL of rapidly stirring methanol. The resulting precipitate was filtered and washed with 50 mL methanol. After dissolving in chloroform, and passed through a short plug of silica gel using chloroform as the eluent. The collected fraction was concentrated *in vacuo* to approximately 10-15 mL and the polymer was precipitated in 200 mL stirring acetone. The polymer was filtered, washed with 50 mL acetone, and dried to yield **P1** as a brilliant yellow solid (459 mg, 87% yield). ^{1}H NMR (400 MHz, $CDCl_3$): δ (ppm) = 7.51 (br. s., 6H), 7.43 (br. s., 4H), 7.07 (br. s., 4H), 6.05 (br. s., 4H), 4.51 (br. s., 4H), 2.26 (br. s., 4H), 1.75 (br. s., 4H), 1.48 (br. s., 4H), 1.33-1.18 (br. m, 76H), 0.90 (br. t., J = 6.9 Hz, 6H). ^{13}C NMR (101 MHz, $CDCl_3$): δ (ppm) = 154.0, 148.3, 145.4, 144.5, 142.5, 123.4, 121.9, 121.3, 118.0, 115.1, 93.6, 91.5, 70.4, 52.4, 34.8, 32.1, 31.8, 30.1, 29.8, 29.5, 26.5, 22.9, 14.3. GPC (THF): M_n = 46 kDa, Đ = 2.1.

*π-Conjugated polymer **P2***

To a 25 mL Schlenk flask equipped with a magnetic stirbar were added **1** (170 mg, 0.242 mmol), **7** (197 mg, 0.242 mmol), $Pd_2(dba)_3$ (5.65 mg, 17.8 μmol), (*p*-tol)$_3$P (7.40 mg, 71.1 μmol), and CuI (2.33 mg, 35.6 μmol). Following 3 vacuum-argon backfill cycles, 7 mL anhydrous degassed toluene and 3 mL anhydrous degassed *N*,*N*-diisopropylamine were added and contents were stirred under argon at room temperature for 20 minutes and then at 65 °C for 2 days. Subsequently, the reaction mixture was stirred at 80 °C for 1 day. The reaction was worked up in the same way as that of **P1** to furnish **P2** as a brilliant orange solid (209 mg, 67% yield). ^{1}H NMR (400 MHz, $CDCl_3$): δ (ppm) = 7.64 (br. s., 4H), 7.50 (br. d., *J* = 7.8 Hz, 4H), 7.08 (br. d., *J* = 7.8 Hz, 4H), 6.36 (br. s., 4H), 4.94 (br. s., 4H), 2.37 (br. s., 4H), 1.85 (br. s., 4H), 1.52 (br. s., 4H), 1.38-1.24 (br. m., 76H), 0.89 (br. t., *J* = 6.6 Hz, 6H). ^{13}C NMR (101 MHz, $CDCl_3$): δ (ppm) = 157.2, 153.3, 148.4, 146.4, 145.4, 145.2, 142.6, 123.5, 122.0, 121.5, 115.3, 108.6, 98.3, 90.4, 75.6, 52.3, 34.8, 32.1, 31.8, 31.4, 30.1-29.9 (br.), 29.6, 26.8, 22.9, 14.3. GPC (THF): M_n = 24 kDa, Đ = 1.7.

III. ^{1}H and ^{13}C NMR Spectra

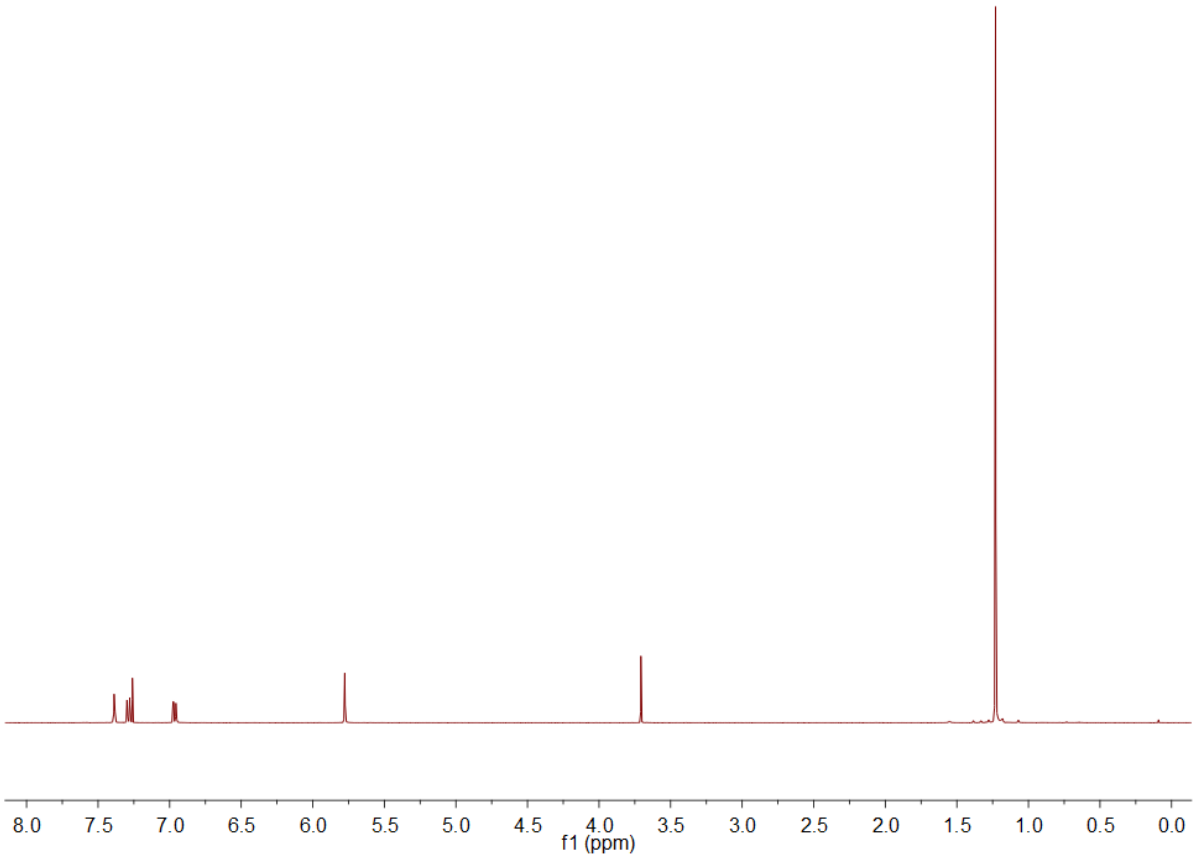

Figure S2. ^{1}H NMR spectrum of **1** (400 MHz, $CDCl_3$).

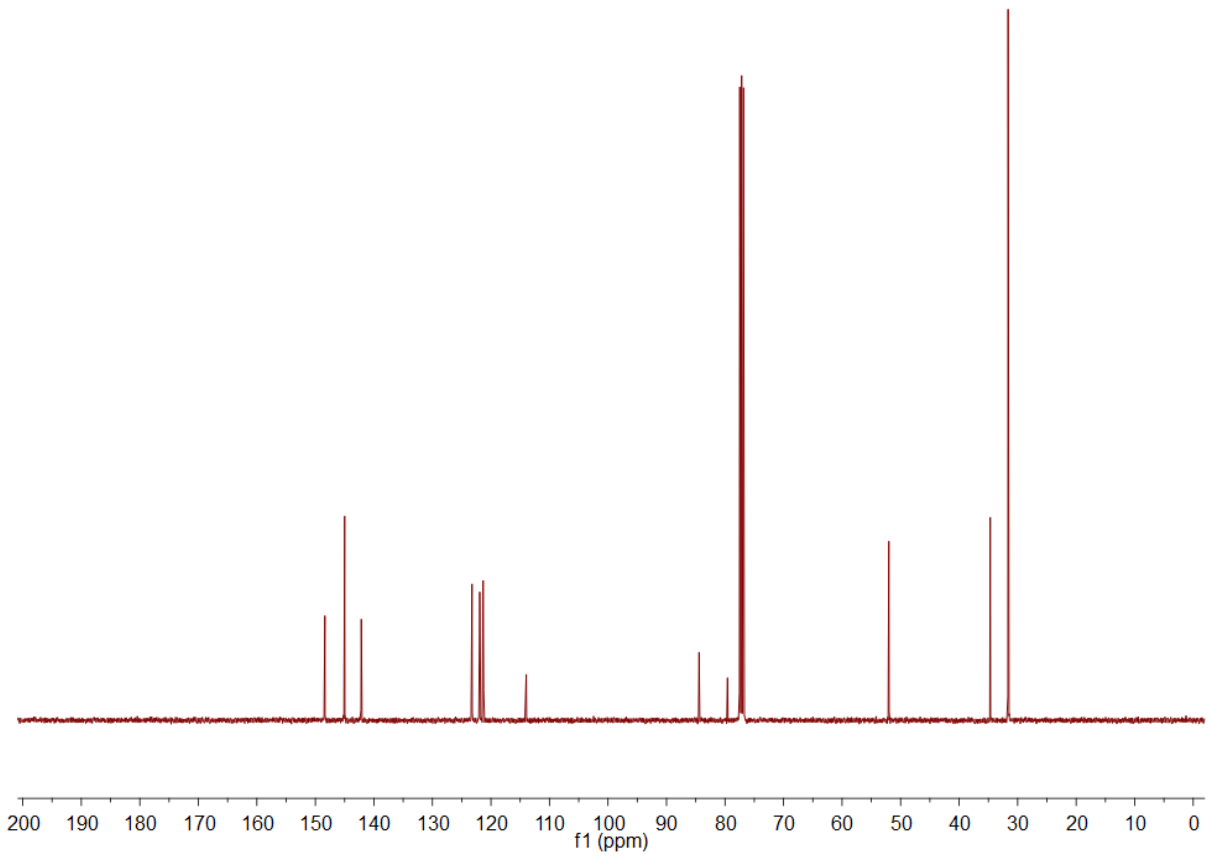

Figure S3. ^{13}C NMR spectrum of **1** (101 MHz, $CDCl_3$).

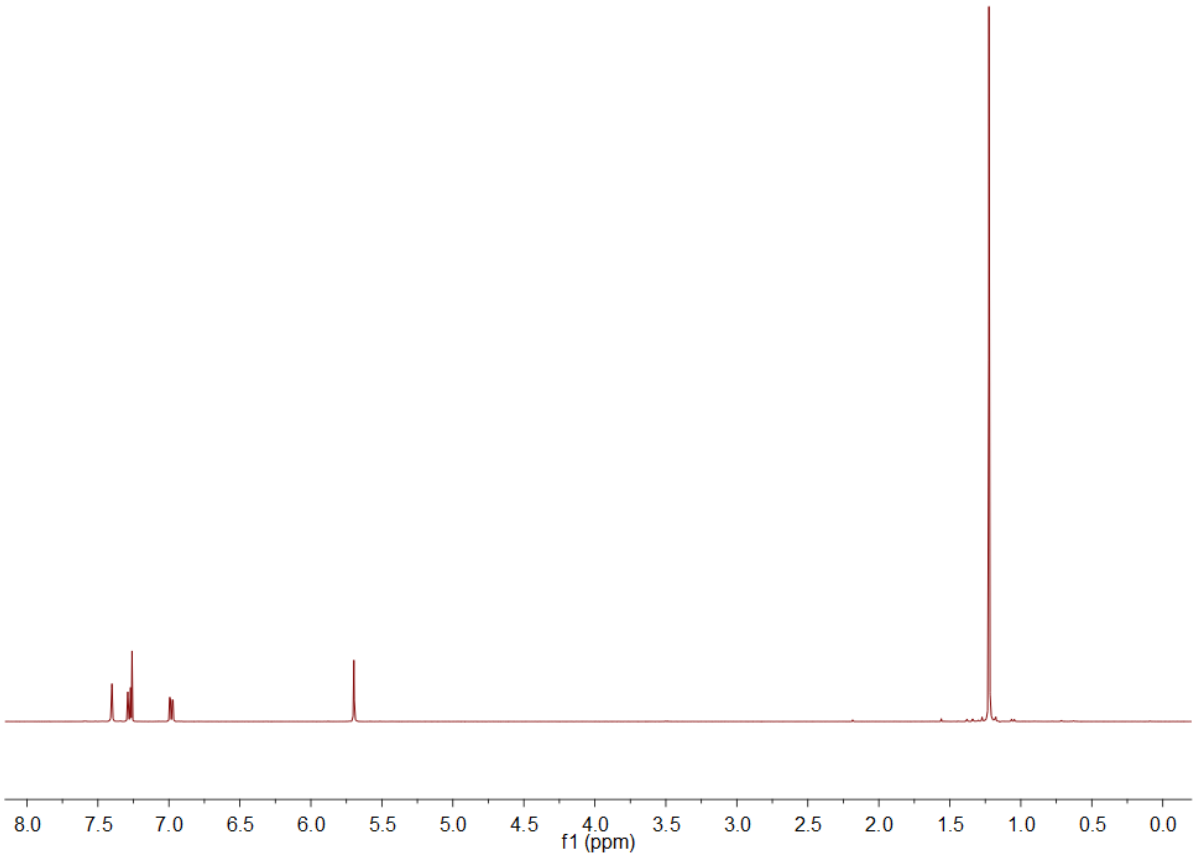

Figure S4. ^{1}H NMR spectrum of **2** (400 MHz, $CDCl_3$).

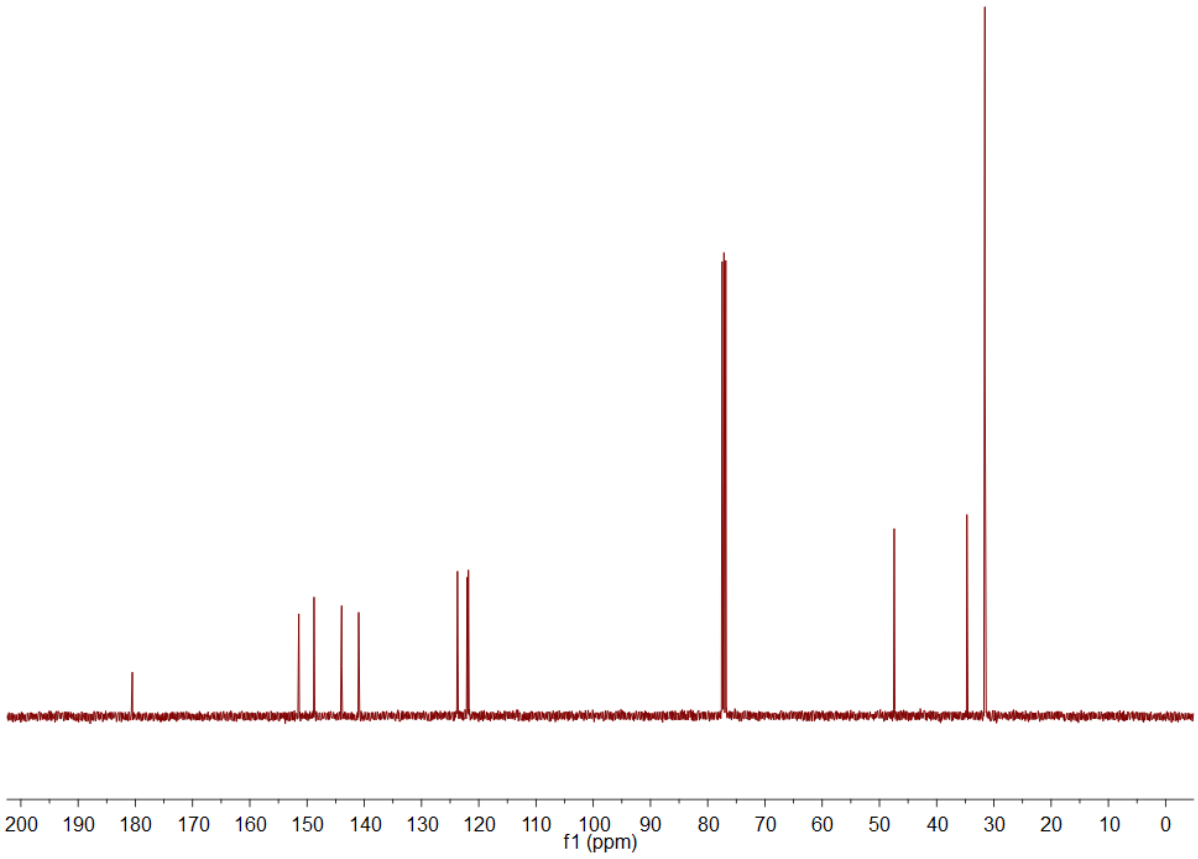

Figure S5. ^{13}C NMR spectrum of **2** (101 MHz, $CDCl_3$).

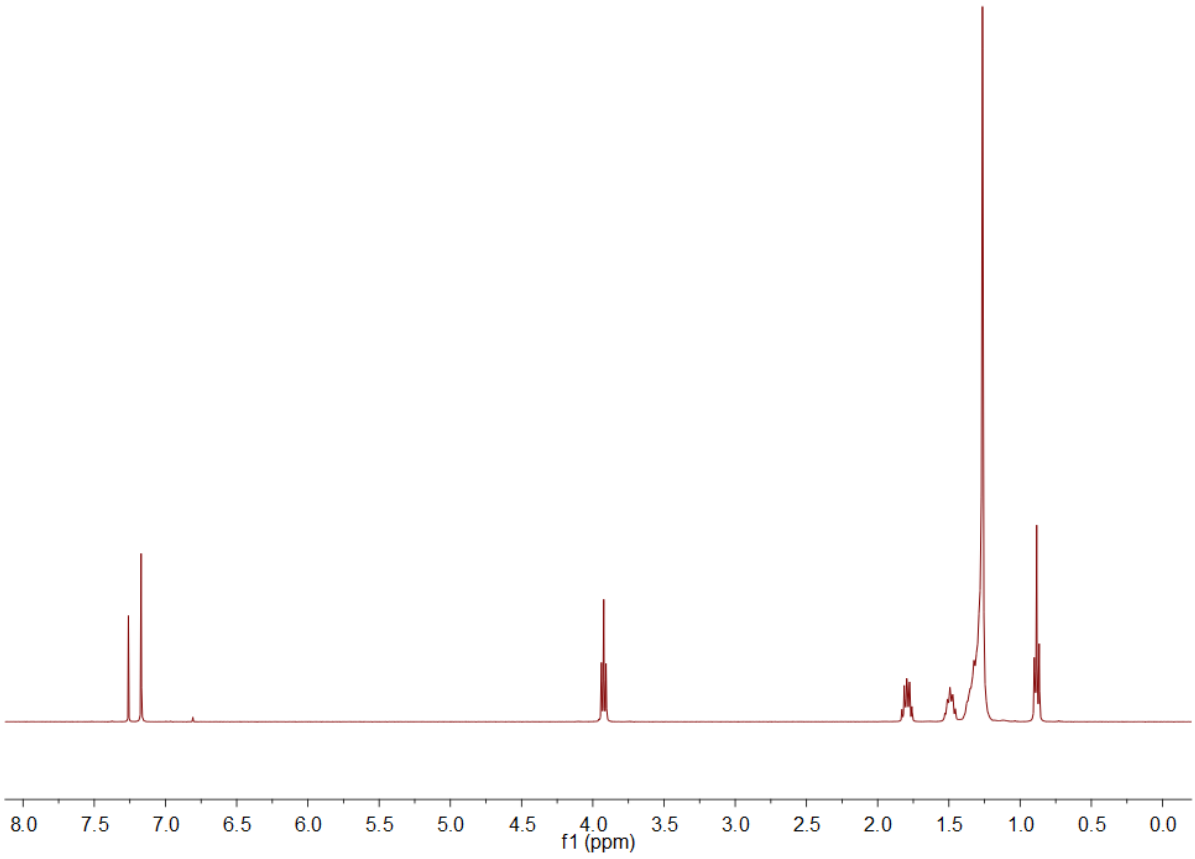

Figure S6. ^{1}H NMR spectrum of **5** (400 MHz, $CDCl_3$).

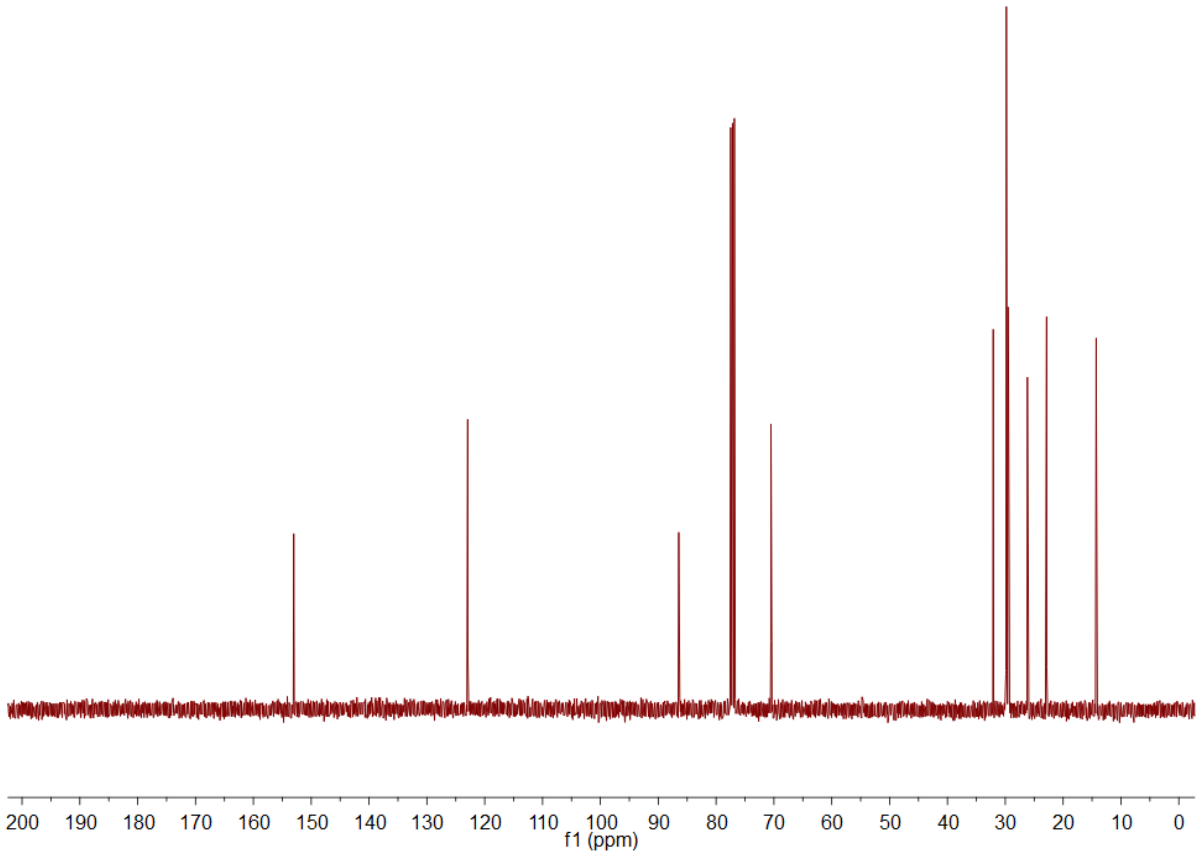

Figure S7. ^{13}C NMR spectrum of **5** (101 MHz, $CDCl_3$).

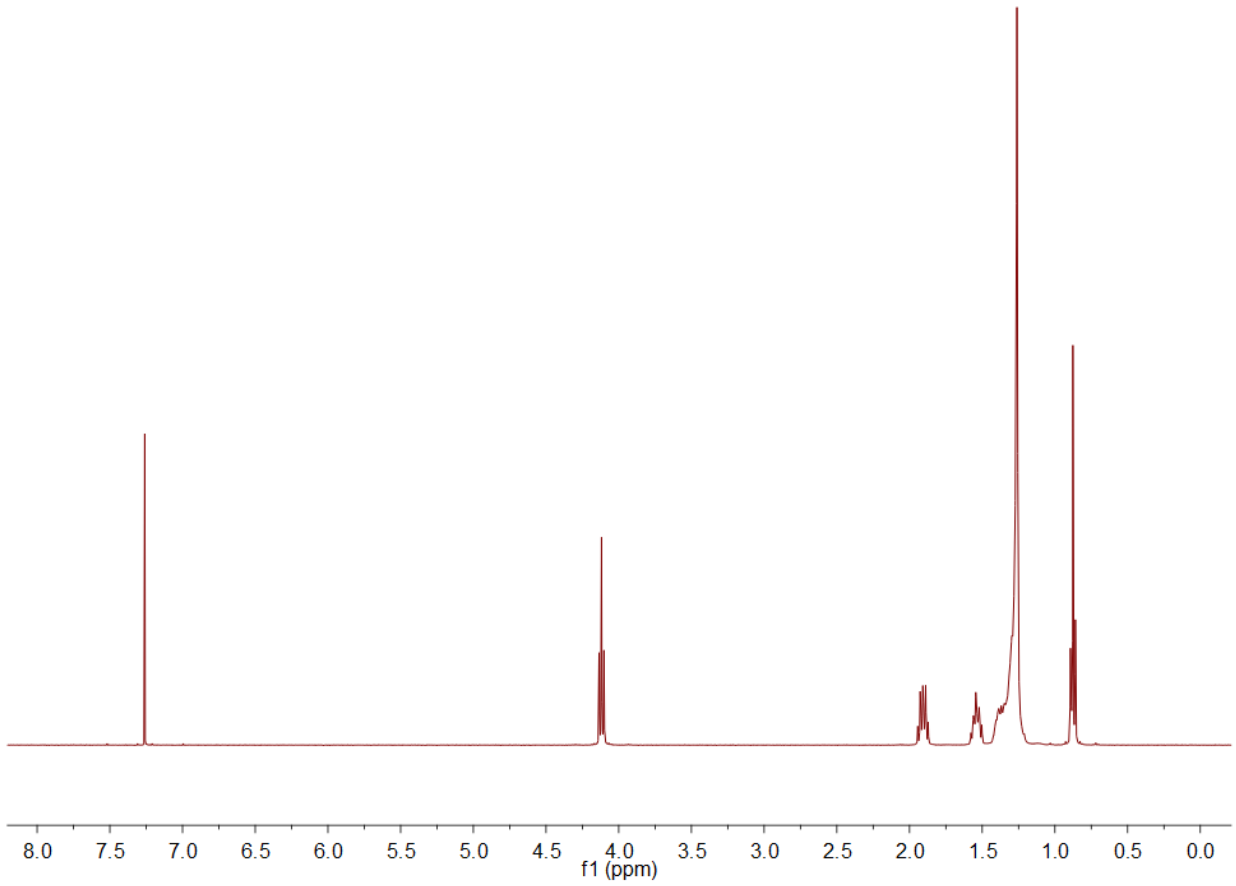

Figure S8. ^{1}H NMR spectrum of **7** (400 MHz, $CDCl_3$).

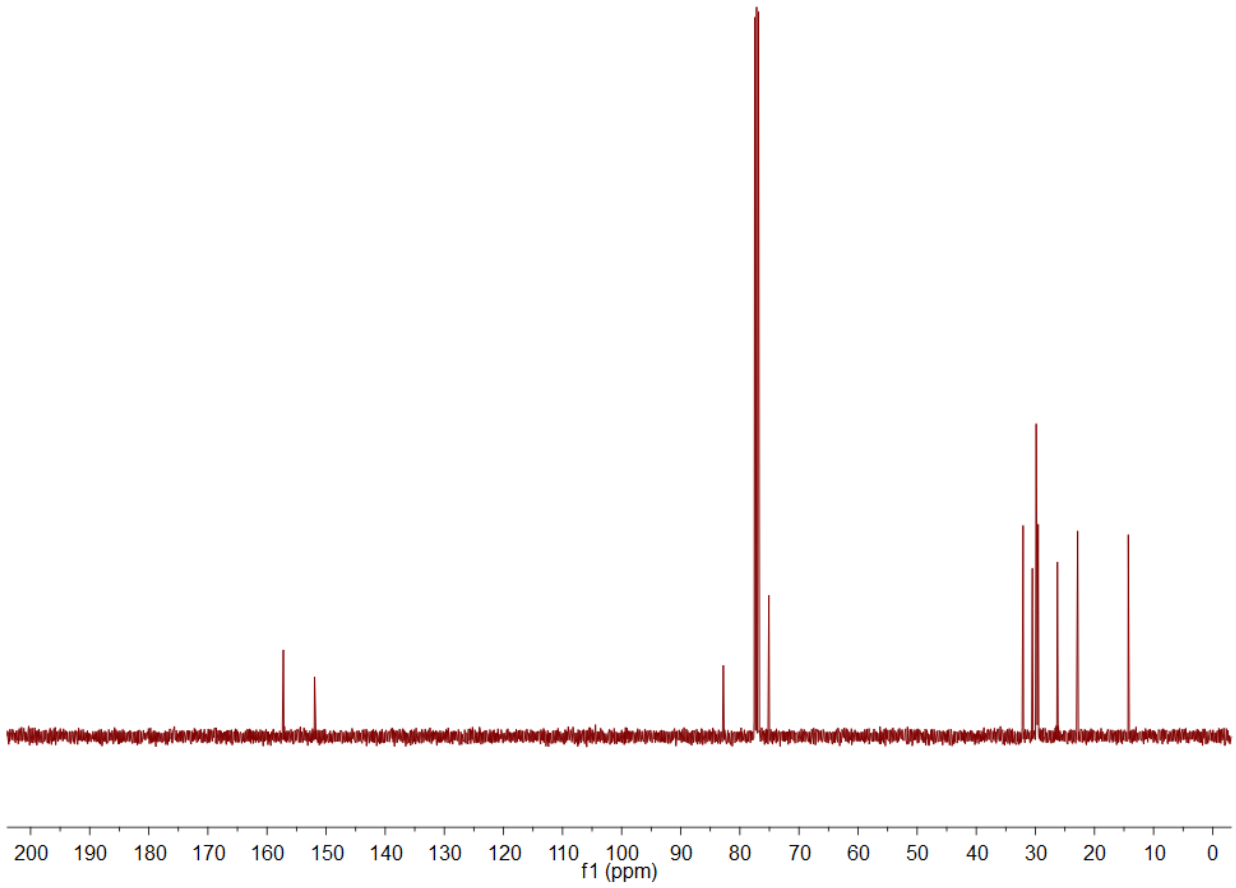

Figure S9. ^{13}C NMR spectrum of **7** (101 MHz, $CDCl_3$).

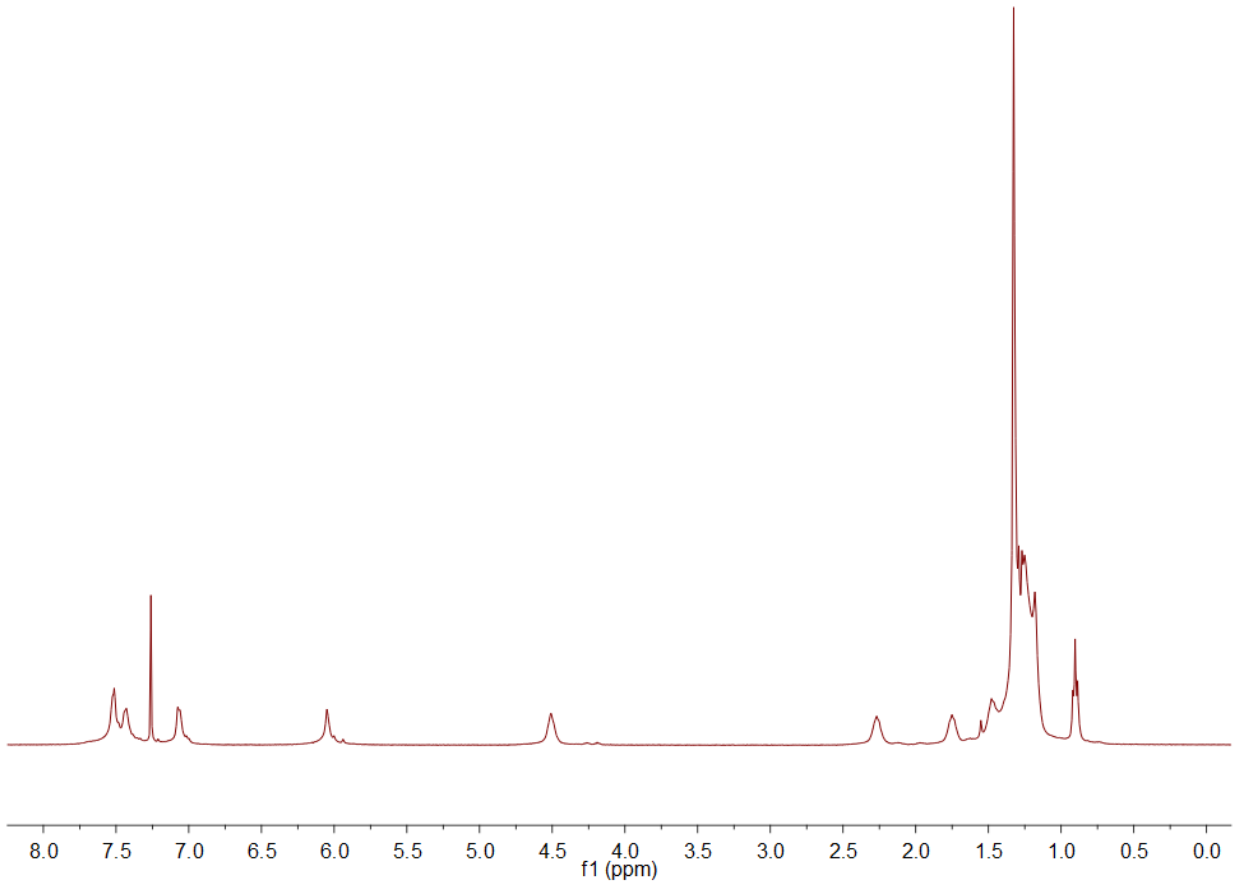

Figure S10. ^{1}H NMR spectrum of **P1** (400 MHz, $CDCl_3$).

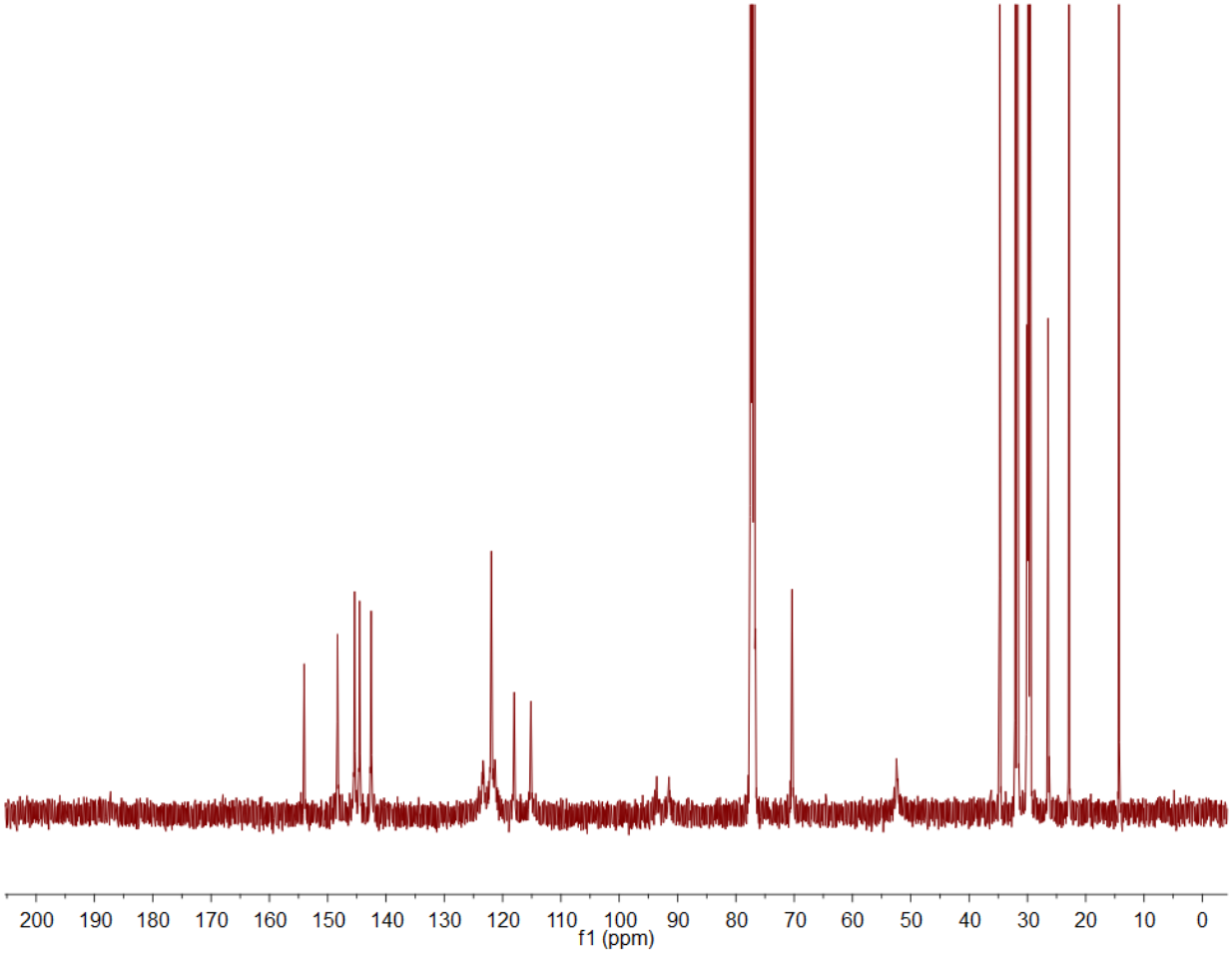

Figure S11. ^{13}C NMR spectrum of **P1** (101 MHz, $CDCl_3$).

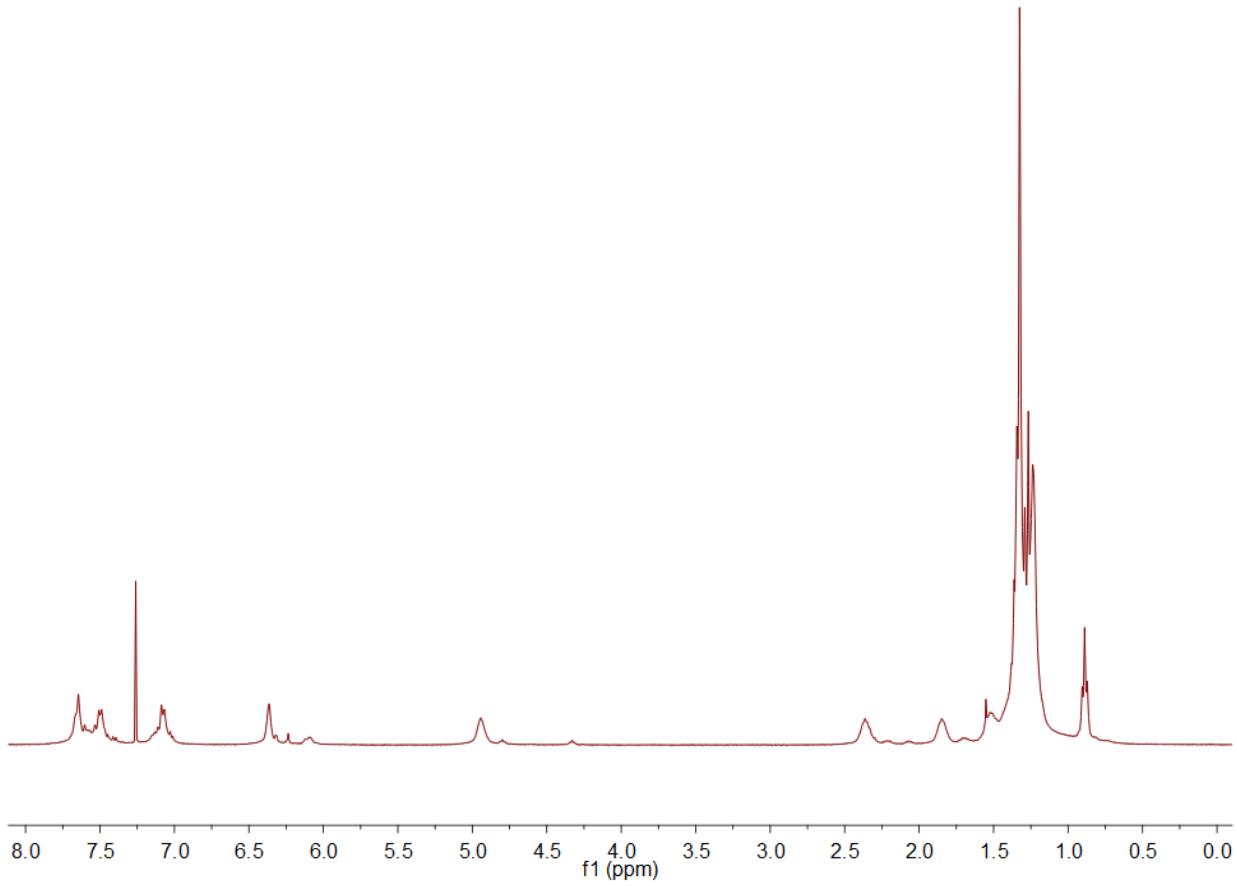

Figure S12. ^{1}H NMR spectrum of **P2** (400 MHz, $CDCl_3$).

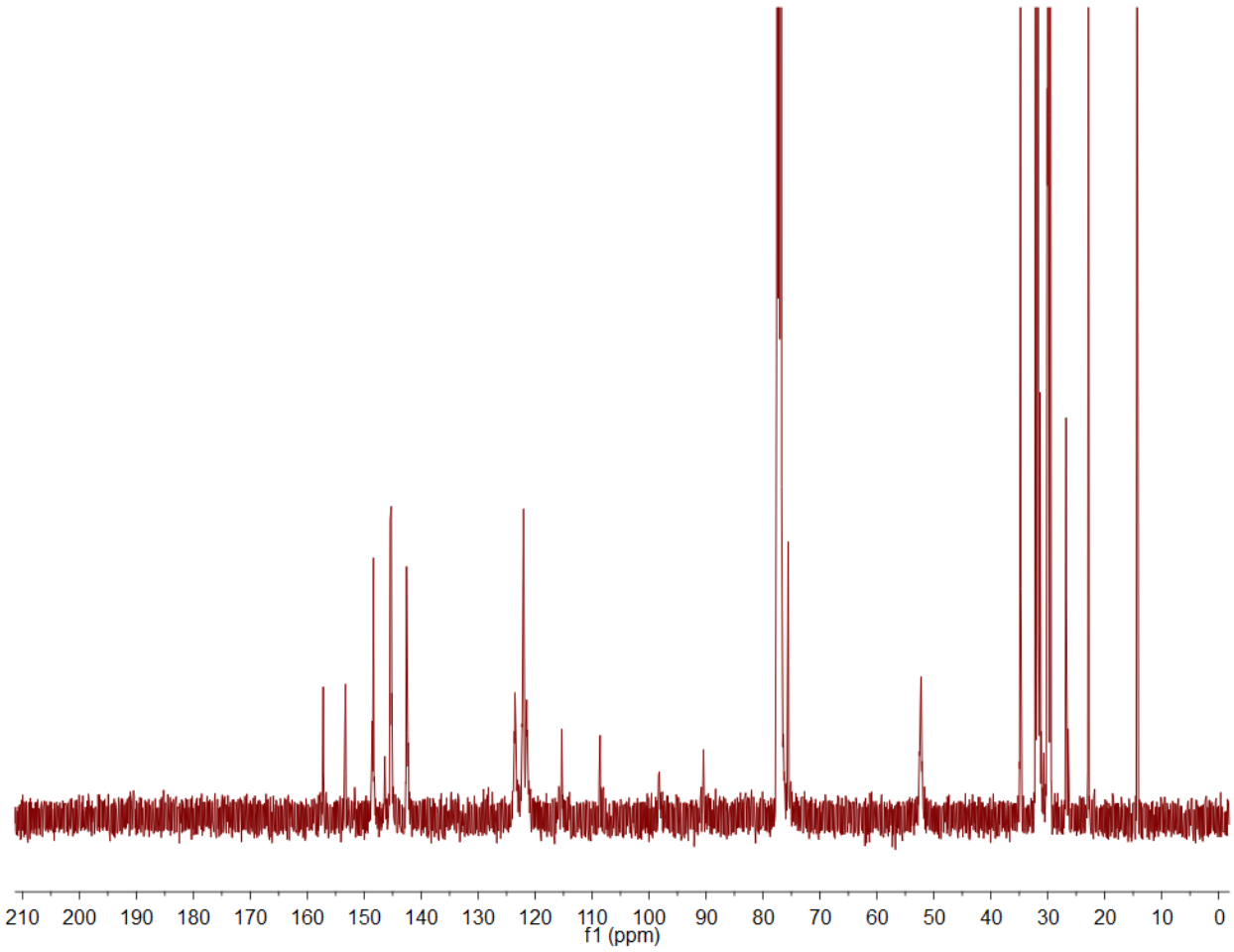

Figure S13. ^{13}C NMR spectrum of **P2** (101 MHz, $CDCl_3$).

IV. Procedure for spectroscopic ellipsometry and data analysis

Ellipsometry data were acquired at a single incident angle of 70° and with a scan range of λ = 192 nm through λ = 994 nm. Samples were coated on a square silicon substrate with facial dimensions 9.9 mm x 9.9 mm and a thickness of 0.525 mm. Before coating, the substrate was initially cleaned with a stream of N_2 gas. A native SiO_2 layer with thickness 6.946 nm was initially determined by the ellipsometer. The analyzed sample consisted of a composite blend of **P1** and **P2** prepared under the same processing conditions as **LSC1**, but with **Red 305** absent. 2.50 mg of **P1** and 2.50 mg of **P2** were dissolved in 0.2 mL of chloroform. 0.1 mL of the resulting solution was spin-casted onto a silicon substrate at 2000 rpm for 45 seconds.

The model used to fit the data to yield the refractive index *n* describes the dielectric constant ε as a function of photon energy *E* and employs a series of harmonic oscillators (Equation S2). This treatment follows the guidance of Campoy-Quiles et al. in their analysis of polyfluorenes and assumes the casted film to be an isotropic layer.[S8]

$$\varepsilon(E) = K + \sum_{j=1}^{N} A_j e^{i\phi_j} \left[\left(E + E_{cj} + i\Gamma_j \right)^{-1} - \left(E - E_{cj} + i\Gamma_j \right)^{-1} \right]$$

Equation S2. Harmonic oscillator model employed in the ellipsometric analysis of the host layer.

Here, *N* is the number of oscillators that obey the model and, for this study, *N* = 7. This value of *N* is the sum of oscillators used to analyze individual polyfluorene-based analogs for **P1** (PFO) and **P2** (F8BT) by Compoy-Quiles et al.[S8] A_j is the amplitude of an oscillator, ϕ_j is the exciton phase, E_{cj} is the corresponding center energy, and Γ_j represents the broadening. A constant *K* accounts for additional transitions in the ultraviolet region. The form of the dielectric function indicated by Equation S2[S9] was used to fit the experimental data (Figures S14 and S15) by employing a Levenberg-Marquardt minimization algorithm. The fit additionally uses the film thickness of the

blend measured via profilometry (i.e. 188.3 nm), which was kept fixed and not fitted by the algorithm. In the region of interest (i.e. λ = 400 – 800 nm), the model (solid line) closely fits the experimental data (dashed line). The mean squared error of the fit is 11.54.

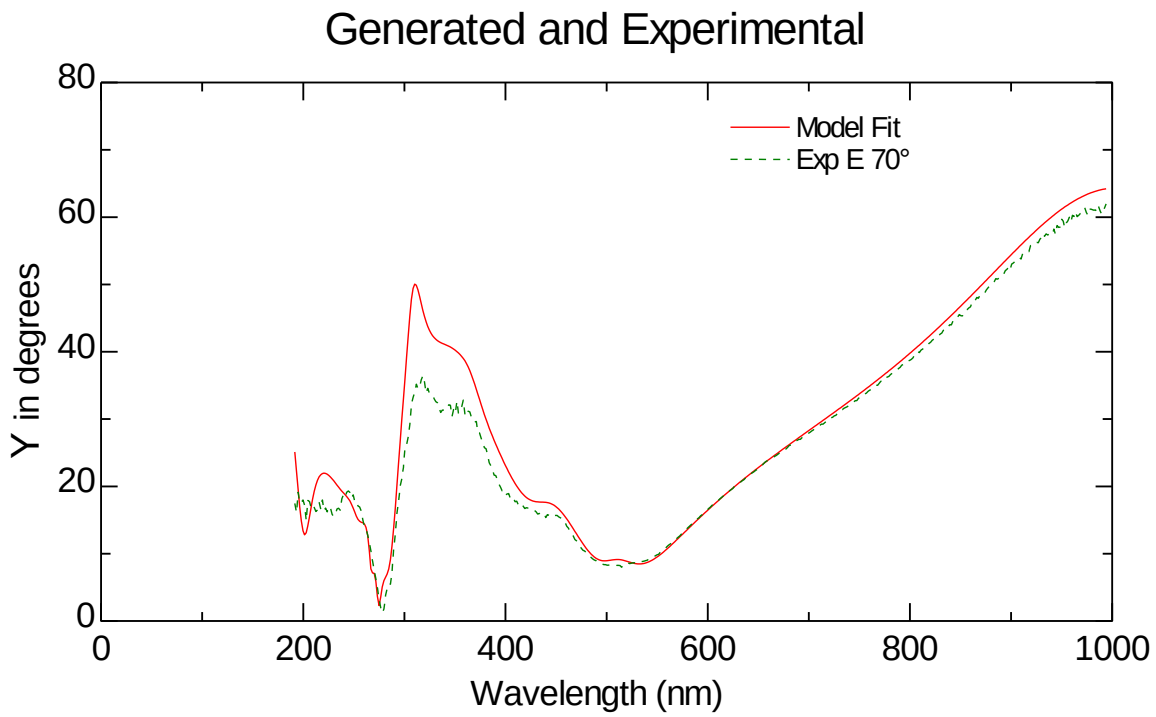

Figure S14. Ellipsometry data for the amplitude ratio Ψ ("Y") and its model fit.

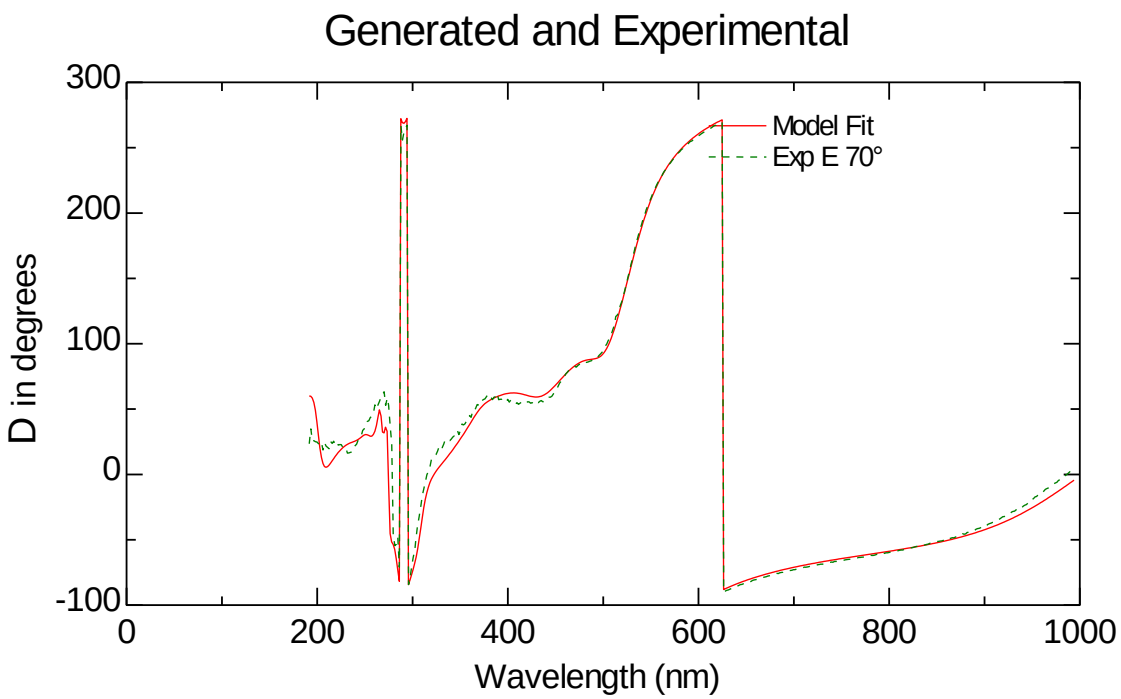

Figure S15. Ellipsometry data for the phase shift Δ ("D") and its model fit.

Parameter	Fitted Value
K	2.2512±0.0264
ϕ_1	5.3288±0.147
A_1	0.052294±0.00642
E_{c1}	2.4452±0.0115
Γ_1	0.21759±0.0209
ϕ_2	-10.117±0.0164
A_2	3.6084±0.976
E_{c2}	4.6051±0.00489

Γ_2	0.42278±0.135
ϕ_3	-0.5264±0.239
A_3	0.091561±0.0219
E_{c3}	2.8239±0.035
Γ_3	0.34234±0.0708
ϕ_4	-19.139±0.459
A_4	1.5969±0.752
E_{c4}	5.1561±0.221
Γ_4	1.2041±0.375
ϕ_5	2.7043±0.858
A_5	0.40926±0.389
E_{c5}	4.1308±0.115
Γ_5	0.628±0.27
ϕ_6	-0.59275±0.596
A_6	3.5452±1.92
Ec_6	4.6408±0.0142
Γ_6	0.40098±0.154
ϕ_7	-4.9983±2.61

A_7	0.33321±1.78
Ec_7	4.6212±0.0492
Γ_7	0.222±0.249

Table S1. Fitted parameters obtained for Equation S1 (N = 7).

In addition to a plot of n with wavelength, the extinction coefficient k, the imaginary component of the complex refractive index $\tilde{n}$ (i.e. $\tilde{n}(\lambda) = n(\lambda) + ik(\lambda)$), was also obtained in the fitting process (Figure S9). The extinction coefficient k is an indication of the extent of absorption by the **P1**:**P2** layer per wavelength and thus bears resemblance to the absorption attributed to **P1** and **P2** in Figure 3a.

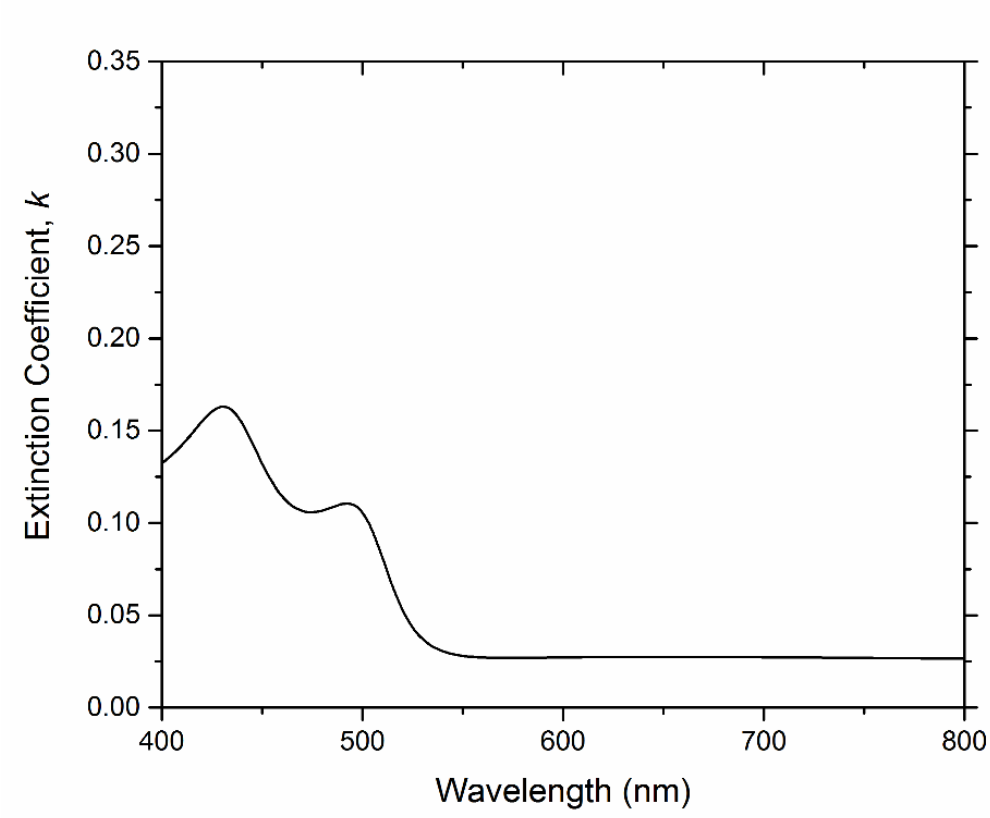

Figure S16. Profile of the extinction coefficient *k* of the analyzed blend composed of **P1** and **P2**.

V. Procedure for Monte Carlo simulation

The Monte Carlo simulation was carried out using an implementation fully described in the supplementary information of a previous report.[S10] Briefly, a photon with a specified wavelength was released into the LSC from the top and it was determined whether the photon was reflected and then whether it was absorbed. If it was absorbed, it was then determined whether the photon was re-emitted, and if so, it was given a wavelength sampled (from the photoluminescence spectrum) and a propagation length and direction. The photon was then allowed to propagate through the device until it was collected or lost. As inputs the program used the absorption and emission spectra of the composite and the refractive index, which, from the ellipsometry data, was approximated to be 1.7 for all wavelengths to simplify the analysis of the LSC by treating it as a symmetric slab waveguide. The slight refractive index difference between the luminescent film and N-SF10 glass was assumed to not significantly influence refractive-index dependent parameters, namely the Fresnel reflection coefficient and trapping efficiency.

To better assess the low reabsorption of the LSC, the absorption spectrum (Figure 3a) used was cut off and corrected at λ = 650 nm due to a slight sinusoidal baseline drift between λ = 650 nm to λ = 800 nm that was attributed to thin film interference effects.[S11,S12] Past λ = 650 nm, all absorptance values were manually set to $1x10^{-4}$. This phenomenon manifests in a regime where no absorption by the LSC is expected and is post-reflection event that should have little to no relevance to the performance analysis.

Once the absorption spectrum was corrected, the photophysical spectra were plotted on a logarithmic scale to clearly view the low extent of reabsorption by the minority **Red 305** (Figure S17).

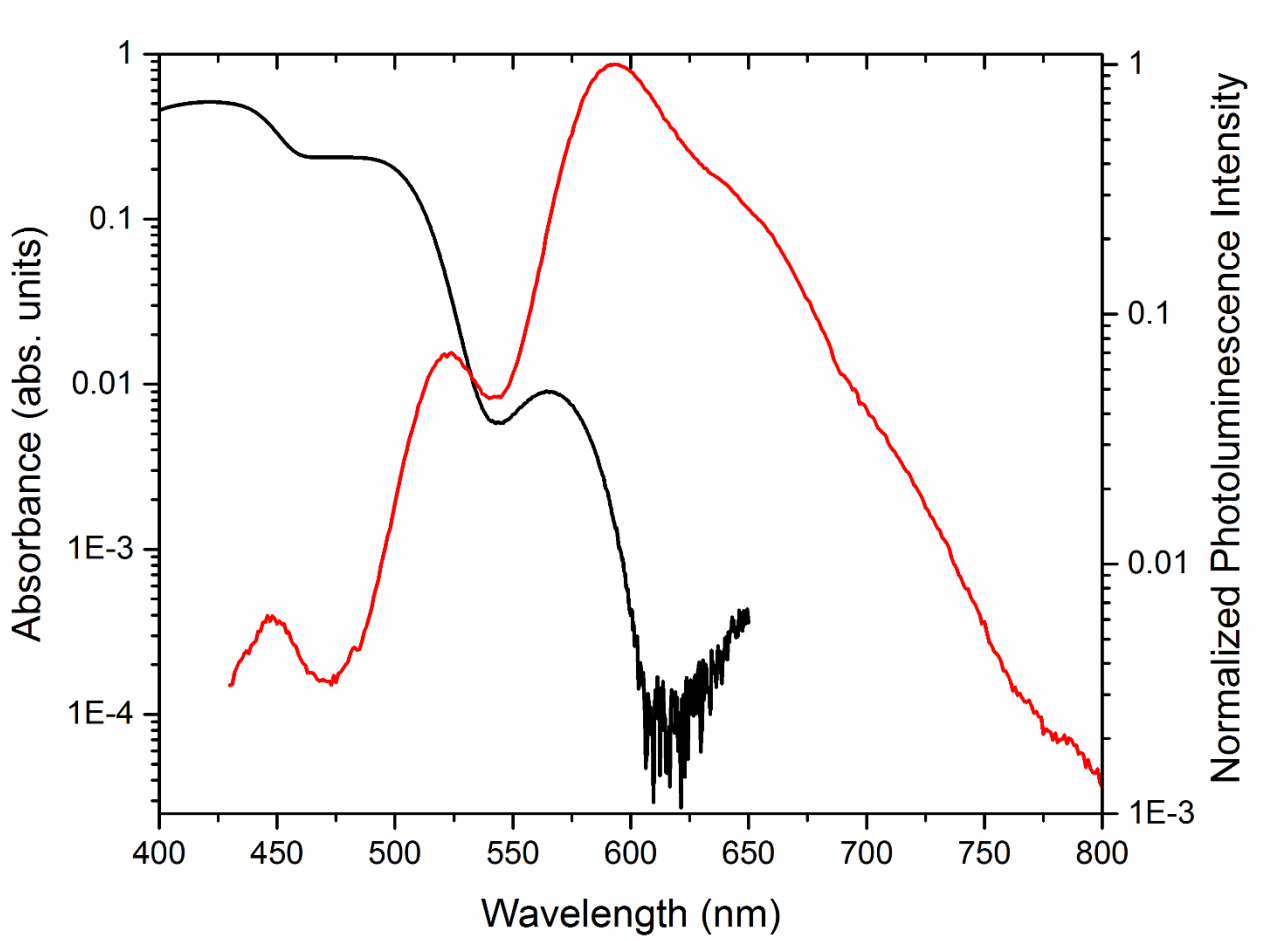

Figure S17. Absorption and emission spectra (logarithmic) of **LSC1** after the specified baseline correction.

VI. References

[S1] P. P. Fu, R. G. Harvey, *J. Org. Chem.* **1977**, *42*, 2407.

[S2] T. M. Long, T. M. Swager, *J. Am. Chem. Soc.* **2003**, *125*, 14113.

[S3] T. M. Swager, C. J. Gil, M. S. Wrighton, *J. Phys. Chem.* **1995**, *99*, 4886.

[S4] J. Bouffard, T. M. Swager, *Macromolecules* **2008**, *41*, 5559.

[S5] E. E. Nesterov, Z. Zhu, T. M. Swager, *J. Am. Chem. Soc.* **2005**, *127*, 10083.

[S6] A slight, but noticeable downfield offset in the chemical shifts was observed in the ^{1}H NMR spectrum with increasing concentration of **1**. Both ^{1}H and ^{13}C NMR spectra are reported for a 20 mg/mL of **1** solution in $CDCl_3$.

[S7] G. Nagarjuna, A. Kokil, J. Kumar, D. Venkataraman, *J. Mater., Chem.* **2012**, *22*, 16091.

[S8] M. Campoy-Quiles, G. Heliotis, R. Xia, M. Ariu, M. Pintani, P. Etchegoin, D. D. C. Bradley, *Adv. Funct. Mater.* **2005**, *15*, 925.

[S9] F. L. Terry, *J. Appl. Phys.* **1991**, *70*, 409.

[S10] I. Coropceanu, M. G. Bawendi, *Nano Lett.* **2014**, *14*, 4097.

[S11] S. E. Burns, N. C. Greenham, R. H. Friend, *Synt. Met.* **1996**, *76*, 205.

[S12] W. M. V. Wan, R. H. Friend, N. C. Greenham, *Thin Solid Films* **2000**, *363*, 310.